

Self-sensing attained in carbon-fiber–polymer-matrix structural composites by using the interlaminar interface as a sensor

Shoukai Wang, Daniel P Kowalik and D D L Chung

Composite Materials Research Laboratory, University at Buffalo, The State University of New York, Buffalo, NY 14260-4400, USA

Received 1 April 2002

Published 4 May 2004

Online at stacks.iop.org/SMS/13/570

DOI: 10.1088/0964-1726/13/3/017

Abstract

Self-sensing is valuable for structural materials, especially those for smart structures. It does not involve the use of embedded or attached sensors, as the structural material is itself the sensor. Self-sensing was attained in carbon-fiber–polymer-matrix structural composites by using the interlaminar interface (i.e., the interface between the laminae of continuous fibers) as a sensor. The attributes sensed were temperature, moisture, damage, and stress. In the case of temperature sensing, the interlaminar interface functioned as either a thermistor or a thermocouple junction. The thermocouple approach required the fibers in the contacting laminae to be dissimilar, whereas the thermistor approach did not. By using two crossply laminae, a two-dimensional array of sensors was attained for spatial distribution sensing.

1. Introduction

Structural materials that exhibit high strength and stiffness are important for satellites, aircraft, automobiles, bicycles, ships, sporting goods, machinery, helicopter rotors, fan blades, wheelchairs, and the civil infrastructure. All of the applications mentioned above, other than those related to the civil infrastructure, require of structural materials low weight for the purposes of fuel economy (in the cases of aircraft, automobiles, bicycles, and ships), functional effectiveness (in the cases of helicopter blades and fan blades), and transportation convenience (in the cases of wheelchairs and machinery).

Polymer-matrix composites containing continuous fibers such as carbon fibers are dominant among lightweight structural materials. Carbon fibers are superior to glass fibers in their low density and high stiffness, although they are higher in cost. On the other hand, the price of carbon fibers has been steadily decreasing in the last few decades, so that carbon fibers have now become cost effective for many applications other than aircraft and satellites. For example, carbon-fiber–polymer-matrix composites are widely used for fishing rods and golf clubs.

A recent direction in structural materials research relates to the development of multifunctional structural materials, i.e., structural materials that serve non-structural functions (such as sensing) while maintaining good structural properties. Multifunctionality means killing two or more birds with one stone, thus reducing cost and simplifying design. This notion is in contrast to that of embedding devices (such as sensors) in a structure so as to attain certain functions. The devices are high in cost and low in durability compared to structural materials. Embedded devices are difficult to repair. Attached devices tend to come off after a period of use. Moreover, embedded devices (such as a strain gage) tend to degrade the mechanical properties of the structure, since they are not designed to function as reinforcements. In addition, an embedded device results in a limited functional volume, so that the multifunctionality occurs only in certain parts of the structure. In contrast, a structural material which is itself multifunctional can eliminate the need for embedded or attached devices, thereby alleviating the problems mentioned above. Therefore, this paper addresses multifunctional lightweight structural materials.

Desirable non-structural functions for a structure depend on the application and include sensing, actuation, energy

generation, energy storage, material removal (for environmental purposes), electromagnetic interference shielding, thermal insulation, etc. This paper is focused on the sensing function, due to its importance in smart structures, which are structures that can sense certain stimuli and respond to the stimuli appropriately—somewhat like human beings, although far less smart than human beings. Sensing is the most basic function of a smart structure, though actuation is a common additional function that provides the response ability. Hence, the multifunctional structural materials addressed in this paper are said to be intrinsically smart—also said to be self-sensing.

Many attributes can be sensed including strain, stress, temperature, moisture, damage, chemical composition, process condition, electromagnetic radiation (such as light), magnetic field, and corrosion. This paper only addresses the sensing of stress (which relates to strain), temperature, moisture, and damage.

Strain sensing is valuable for structural vibration control, as vibration is a form of strain and vibration sensing in conjunction with vibration suppression is needed to achieve vibration control. Vibration control is required for any structure, particularly those to which optical components are attached. Vibration control leads to performance improvement, hazard mitigation, and noise reduction.

Temperature sensing is valuable since temperature can affect the operation of a structure and thermal control is useful for energy conservation, operation control, and hazard mitigation.

Moisture sensing is valuable since moisture can affect the performance of a polymer-matrix composite, particularly when the polymer is epoxy. Humidity control is also useful for operation control.

Damage sensing pertains to structural health monitoring. Composite components that are manufactured under the same conditions can differ in the degree of fiber alignment, the quality of the fiber–matrix interface and the distribution of flaws. Therefore, the useful lifetime of a composite component is a variable quantity which cannot be predicted accurately based on past experience in using similar components. As a result, damage sensing is needed to determine the amount of remaining service life of a component. Due to the aging of aircraft and the occurrence of the AA587 aircraft crash in Queens, NY, in November 2001, structural health monitoring has become critically important to carbon-fiber–polymer-matrix composites. In general, damage can be due to mechanical or thermal abuse. Both mechanical and thermal forms of damage are addressed in this paper.

The dominant polymer matrix for carbon-fiber–polymer-matrix composites is epoxy—a thermoset. Therefore, this paper addresses mainly carbon-fiber–epoxy-matrix composites, although carbon-fiber–thermoplastic-matrix composites are addressed to a limited extent.

The science behind stress/strain sensing pertains to the use of a measurable quantity to indicate the stress/strain. The quantity is commonly the electrical resistance (in the case of a resistive or piezoresistive sensor) or a voltage (in the case of a piezoelectric sensor). A resistive sensor functions by the change in resistance (not resistivity) upon straining. A piezoresistive sensor functions by the change in resistivity upon straining. A piezoelectric sensor functions by the

generation of a voltage that relates to the strain. In the case of an optical fiber sensor, the relevant quantities are the intensity and phase of the light. However, an optical fiber is not a structural material.

This paper addresses the use of the electrical resistance measurement to sense temperature, moisture, stress, and damage. For temperature sensing, an additional quantity used for sensing is the voltage, as generated by the Seebeck effect (a thermoelectric effect in which a voltage results from a temperature gradient in a material). A thermoelectric device based on the change of the electrical resistivity with temperature is known as a thermistor. One based on the Seebeck effect is a thermocouple. This paper provides thermistors and thermocouples in the form of carbon-fiber structural composites.

The electrical resistance of a continuous carbon fiber is much higher in the longitudinal (fiber) direction than in the through-thickness direction. The resistances in both directions are used in this work for the purpose of sensing. In addition, the effect of processing condition (specifically the curing pressure during composite fabrication) on the through-thickness resistance is addressed. Furthermore, the contact electrical resistivity of the interface between laminae is used in this work as a quantity that gives information on the structure of this interface. This interface (referred to as the interlaminar interface) is critical to the mechanical integrity of a structural composite, since delamination is the most common type of defect in these composites. The contact resistance contributes to the through-thickness resistance of a composite.

Previous work on the self-sensing of carbon-fiber–polymer-matrix composites used a volume of the composite as the sensor [1–17]. In particular, the volume electrical resistivity of the composite was used as the indicator of quantities such as strain and damage. The resistivity in the longitudinal (fiber) direction was used to indicate damage in the form of fiber breakage; that in the through-thickness direction was used to indicate damage in the form of delamination [10–17]. The resistivities in both directions were also used to indicate strain in the longitudinal direction, as the strain caused the degree of fiber alignment to increase, thereby decreasing the resistivity in the longitudinal direction and increasing that in the through-thickness direction [10–17].

In contrast to previous work [1–17], this work used the interlaminar interface as the sensor. The attraction of this method lies in the fact that there can be subdivisions of an interlaminar interface, as in the case of a two-dimensional array of junctions of two crossply laminae, with each junction involving the overlap of a group of fibers of one lamina with a group of fibers in the adjacent lamina (figure 1). Thus, two laminae alone provide an array of sensors. The array provides information on the spatial distribution of the attribute sensed. In contrast, the use of a volume of the composite as the sensor is less amenable to spatial distribution sensing, due to the relatively large minimum size for each unit of volume for the attaching of electrical contacts.

In this paper, the interlaminar interface was used as a thermistor, a thermocouple junction, a stress sensor, a damage sensor, and a moisture sensor. Spatial distribution sensing was also demonstrated. The interlaminar interface investigated was as ordinarily made in conventional composite processing.

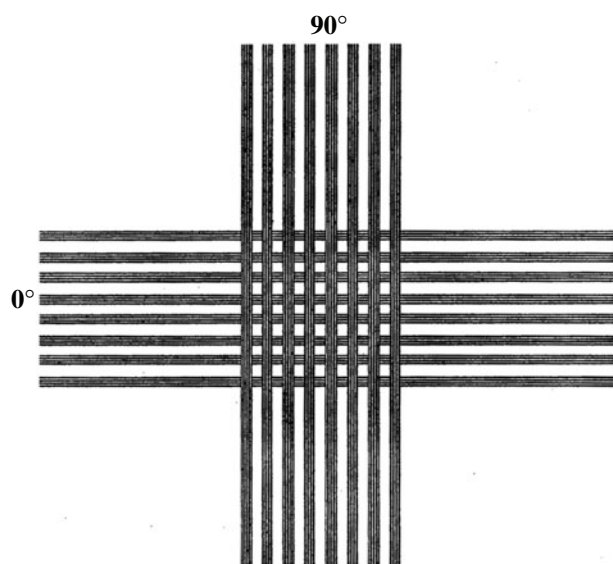


Figure 1. Sensor array in the form of a carbon-fiber–polymer-matrix composite comprising two crossply laminae.

No modification was made to the interface. Thus, the sensing technology provided is applicable to conventional composites.

2. Interlaminar interface as a thermistor

2.1. Introduction

A polymer-matrix composite comprising layers (laminae) of continuous fibers tends to be mechanically weakest at the interface between the laminae. As a result, delamination is a common mechanism of failure in the composites. The study of the interlaminar interface has been previously performed by measuring the interlaminar shear strength (ILSS) by techniques such as the short-beam method [18], the Iosipescu method [19], and other methods [20]. Although ILSS is a valuable quantity that describes the mechanical property of the joint between laminae, it gives little information on the interfacial structure, such as the extent of direct contact (without the polymer matrix in between) between fibers of adjacent laminae and the residual interlaminar stress resulting from the anisotropy between adjacent laminae. The anisotropy is severe when the fibers in the adjacent laminae are in different directions, since the fibers and polymer matrix differ greatly in modulus and thermal expansion coefficient. Direct contact between fibers of adjacent laminae occurs due to the flow of the matrix during composite fabrication and the waviness of the fibers. Direct contact means that the thickness of the matrix between the adjacent fibers is so small (say, a few ångströms) that electrons can tunnel or hop from one fiber to the other. The presence of direct contact has been shown by the fact that the volume electrical resistivity of carbon-fiber–epoxy-matrix composites in the through-thickness direction is finite, even though the epoxy matrix is electrically insulating [12].

In contrast to previous work, this section uses the contact electrical resistivity of the interlaminar interface as a quantity to describe the structure of this interface. Note that the volume electrical resistivity is a geometry-independent quantity that describes the resistivity of a three-dimensional material in a

Table 1. Carbon-fiber and epoxy-matrix properties (according to ICI Fiberite).

10E—Torayca T-300 (6K) untwisted, UC-309 sized	
Diameter	7 μm
Density	1.76 g cm^{-3}
Tensile modulus	221 GPa
Tensile strength	3.1 GPa
976 Epoxy	
Process temperature	350 °F (177 °C)
Maximum service temperature	350 °F (177 °C) dry 250 °F (121 °C) wet
Flexural modulus	3.7 GPa
Flexural strength	138 MPa
T_g	232 °C
Density	1.28 g cm^{-3}

particular direction. For example, the volume resistivity of a composite in the through-thickness direction reflects both the volume resistance within each lamina in the through-thickness direction and the contact resistance at each interlaminar interface. Hence, the volume resistivity does not simply relate to the structure of the interlaminar interface. However, the contact resistivity does, since it is a geometry-independent quantity that describes the resistivity of a plane in the direction perpendicular to the plane. The volume resistivity has the unit $\Omega \text{ cm}$ whereas the contact resistivity has the unit $\Omega \text{ cm}^2$.

For a composite with electrically conductive fibers, such as carbon fibers, and an electrically insulating matrix, such as epoxy, the contact resistivity can be conveniently measured, since the fibers serve as electrical leads. The contact resistivity is lower when the extent of direct contact between fibers of adjacent laminae is greater. However, the contact resistivity also depends on the nature of each direct contact. This nature is reflected by the activation energy for electrons to jump from one lamina to an adjacent one. This activation energy is expected to be affected by the interlaminar stress. It can be determined by measuring the temperature dependence of the contact resistivity, as it is related to the slope (negative) of the Arrhenius plot of the logarithm of the contact conductivity (conductivity being the reciprocal of the resistivity) versus the inverse of the absolute temperature. The jumping of the electrons from one lamina to another is a thermally activated process, so the higher is the temperature, the higher is the contact conductivity. The contact resistivity and the activation energy are quantities determined in this section for the purpose of characterizing the interlaminar interface.

2.2. Experimental methods

Two laminae of unidirectional carbon-fiber–epoxy-matrix prepregs (provided by ICI Fiberite) (table 1) in the form of strips, with one strip on top of the other (figure 2), were fabricated into a composite at the overlapping region (6 mm \times 6 mm) of the two laminae by applying pressure and heat to the overlapping region (without a mold). For the unidirectional junction, the area of the junction was defined by the use of electrically insulating paper in the interlaminar space outside the junction area. The pressure was provided by a weight, which was varied in order to vary the pressure. A glass-fiber–epoxy-matrix composite spacer was placed between the

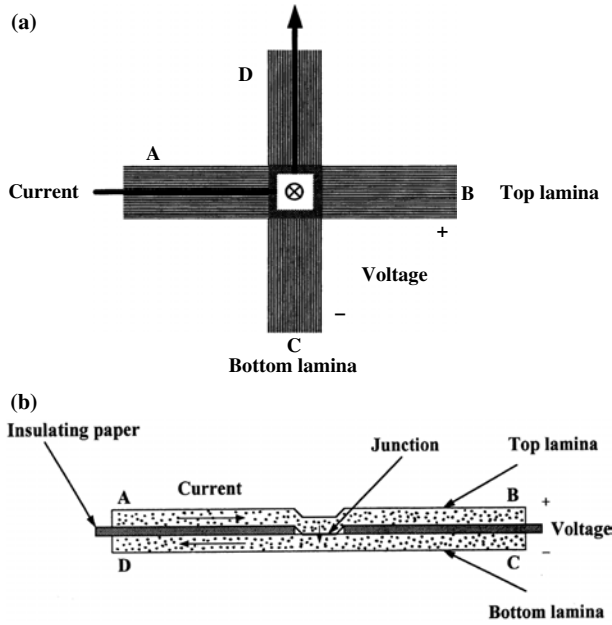


Figure 2. Composite configurations for testing contact resistivity as a function of temperature. (a) Crossply, (b) unidirectional.

weight and the junction (the overlapping region of the two strips). The heat was provided by a Carver hot press. A Watlow model 981C-10CA-ARRR temperature controller was used to control the temperature and the ramping rate. Each of the samples was put between the two heating platens of the hot press and heated linearly up to $175 \pm 2^\circ\text{C}$ at the rate of $2.5^\circ\text{C min}^{-1}$. Then it was cured at that temperature for 10 h and subsequently cooled linearly to $50 \pm 2^\circ\text{C}$ at the rate of $0.18^\circ\text{C min}^{-1}$. After that the sample was reheated up to $150 \pm 2^\circ\text{C}$ and then cooled back to $50 \pm 2^\circ\text{C}$. Both the reheating and the subsequent cooling were linear and at the rate of $0.15^\circ\text{C min}^{-1}$. After the reheating and cooling, the sample was heated linearly up to $150 \pm 2^\circ\text{C}$ again at the rate of 1°C min^{-1} and then cooled linearly back to $50 \pm 2^\circ\text{C}$ at the rate of $0.15^\circ\text{C min}^{-1}$.

All the time, the contact electrical resistance and the temperature of the sample were measured respectively by a Keithley 2001 multimeter and a T-type thermocouple, which was put just beside the junction. Electrical contacts were made to the four ends of the two strips, so as to measure the contact electrical resistivity (resistance multiplied by contact area, which is the area of the overlapping region) between the two laminae in the composite, using the four-probe method (figure 2). The epoxy at the ends of each prepreg strip was burned out to expose the carbon fibers for the purpose of making electrical contacts. These exposed fibers were wrapped by pieces of copper foil, with silver paint between the copper foil and the fibers. The electric current flowed from A to D, such that the dominant resistance was the contact resistance, as the volume resistance of the strips was negligible in comparison. The voltage between B and C is the voltage between the two laminae.

2.3. Results and discussion

The current-voltage characteristic is linear for all samples studied. Figure 3 shows the variation of the contact

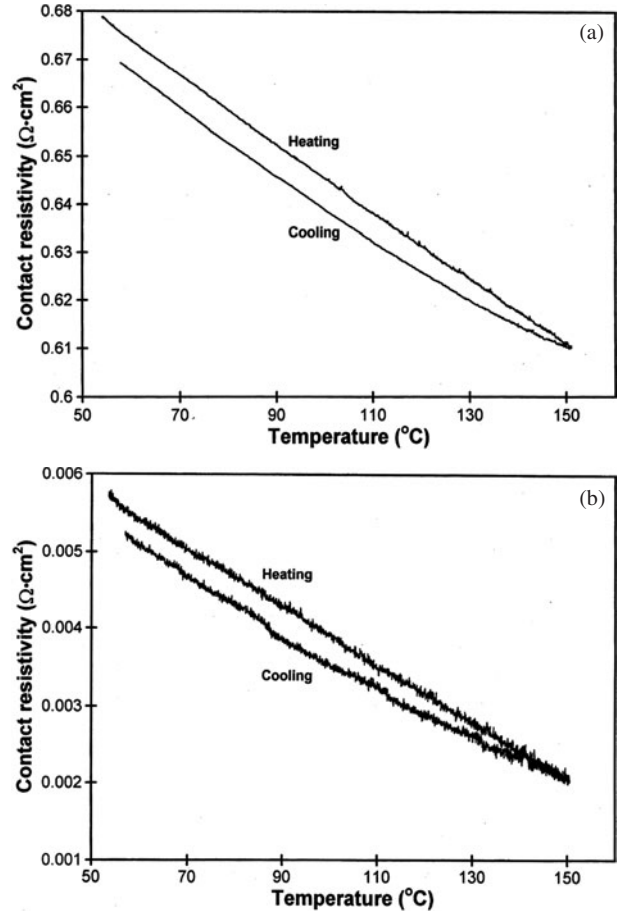


Figure 3. Variation of contact electrical resistivity with temperature during heating and cooling at $0.15^\circ\text{C min}^{-1}$ for (a) sample made without any curing pressure and (b) sample made with a curing pressure of 0.33 MPa.

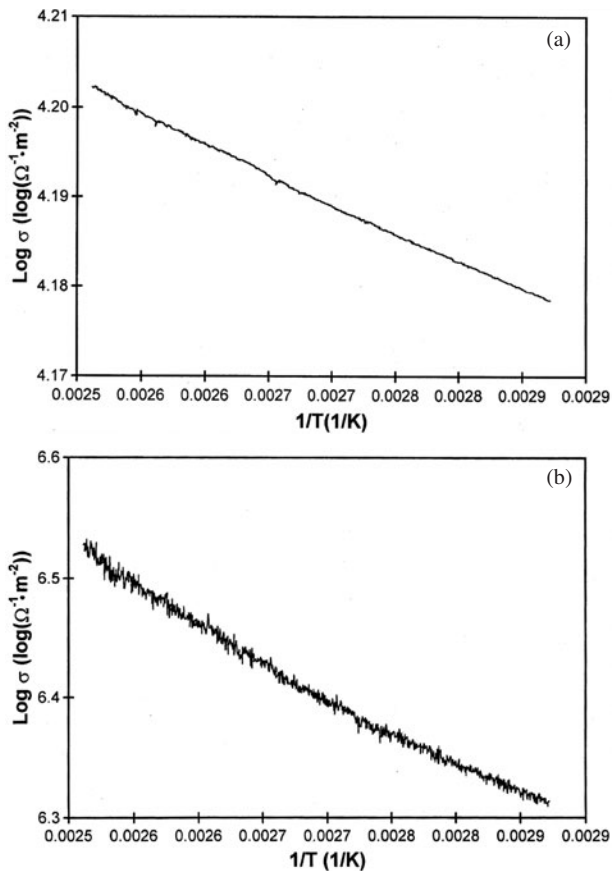
resistivity ρ_c with temperature during reheating and subsequent cooling, both at $0.15^\circ\text{C min}^{-1}$, for samples cured at 0 and 0.33 MPa. The corresponding Arrhenius plots of log contact conductivity (inverse of contact resistivity) versus inverse absolute temperature during heating are shown in figure 4. From the slope (negative) of the Arrhenius plot, which is quite linear, the activation energy can be calculated by using the equation

$$\text{Slope} = -\frac{E}{2.3k} \quad (1)$$

where k is the Boltzmann constant, T is the absolute temperature (in K) and E is the activation energy. The linearity of the Arrhenius plot means that the activation energy does not change throughout the temperature variation. This activation energy is the energy for an electron jumping from one lamina to the other. Electronic excitation across this energy enables conduction in the through-thickness direction. This activation phenomenon is common in the electrical conduction of composite materials with an insulating matrix and an electrically conducting filler (whether particles or fibers). Based on volume resistivity measurement, an activation energy in the range from 0.060 to 0.069 eV has been previously reported for short carbon-fiber-polymer-matrix composites [21]. Direct measurement of the contact resistivity is impossible for the short fiber composites.

Table 2. Activation energy for various composites. The standard deviations are shown in parentheses.

Composite configuration	Curing pressure (MPa)	Composite thickness (mm)	Contact resistivity ρ_{co} ($\Omega \text{ cm}^2$)	Activation energy (eV)		
				Heating at $0.15^\circ\text{C min}^{-1}$	Heating at 1°C min^{-1}	Cooling at $0.15^\circ\text{C min}^{-1}$
Crossply	0	0.36	0.73	0.0131 (2×10^{-5})	0.0129 (3×10^{-5})	0.0125 (8×10^{-6})
Crossply	0.062	0.32	0.14	0.0131 (4×10^{-5})	0.0127 (7×10^{-5})	0.0127 (4×10^{-5})
Crossply	0.13	0.31	0.18	0.0168 (3×10^{-5})	0.0163 (4×10^{-5})	0.0161 (2×10^{-5})
Crossply	0.19	0.29	0.054	0.0222 (3×10^{-5})	0.0223 (3×10^{-5})	0.0221 (1×10^{-5})
Crossply	0.33	0.26	0.0040	0.118 (4×10^{-4})	0.129 (8×10^{-4})	0.117 (3×10^{-4})
Unidirectional	0.42	0.23	0.29	0.0106 (3×10^{-5})	0.0085 (4×10^{-5})	0.0081 (2×10^{-5})

**Figure 4.** Arrhenius plot of log contact conductivity versus inverse absolute temperature during heating at $0.15^\circ\text{C min}^{-1}$ for (a) sample made without any curing pressure and (b) sample made with a curing pressure of 0.33 MPa.

A slightly concave shape is present in the Arrhenius plots obtained during heating as well as cooling (figure 4). This shape means that the activation energy increases slightly with increasing temperature. On the other hand, the interlaminar thermal stress decreases with increasing temperature, as explained in the next paragraph. Thus, this curvature cannot be explained by considering the effect of the thermal stress on the activation energy. The origin of the curvature is currently not clear.

The activation energies, thicknesses, and room temperature contact resistivities for samples made at different curing pressures and composite configurations are shown in table 2. All the activation energies were calculated based on the data at $75\text{--}125^\circ\text{C}$. In this temperature regime, the temperature change was very linear and well controlled. From table 2 it can be seen that, for the same composite configuration (crossply), the higher the curing pressure, the smaller the composite thickness (because of more epoxy being squeezed out), the lower the contact resistivity, and the higher the activation energy. A smaller composite thickness corresponds to a higher fiber volume fraction in the composite. During curing and subsequent cooling, the matrix shrinks while the carbon fibers essentially do not, so a longitudinal compressive stress will develop in the fibers. For carbon fibers, the modulus in the longitudinal direction is much higher than that in the transverse direction. Moreover, carbon fibers are continuous in the longitudinal direction, but discontinuous in the transverse direction. Thus, the overall shrinkage in the longitudinal direction tends to be less than that in the transverse direction. Therefore, there will be a residual interlaminar stress in the two crossply layers in a given direction. This stress accentuates the barrier for the electrons to jump from one lamina to the other. The greater the residual interlaminar stress, the higher the barrier, which is the activation energy. After curing and subsequent cooling, heating will decrease the thermal stress, due to the CTE (coefficient of thermal expansion) mismatch between fibers and matrix. Both the thermal stress and the curing stress contribute to the residual interlaminar stress. Therefore, the higher the curing pressure, the larger the fiber volume fraction, the greater the residual interlaminar stress, and the higher the activation energy, as shown in table 2.

The activation energy increased gradually with increasing curing pressure from 0 to 0.19 MPa, but increased abruptly from 0.02 to 0.12 eV when the curing pressure was increased from 0.02 to 0.12 MPa. The abrupt increase at high pressure is probably not due to the interlaminar stress abruptly increasing, but is probably due to another phenomenon that occurred at the high curing pressure of 0.33 MPa. This phenomenon has not been investigated, but one possibility is the pressure increasing the anisotropy of the matrix and thereby accentuating the barrier for electron jumping from one lamina to the other.

The curing pressure for the sample in the unidirectional composite configuration was higher than that of any of the crossply samples (table 2). Consequently, the thickness was the lowest. As a result, the fiber volume fraction was the highest. However, the contact resistivity of the unidirectional sample was the second highest rather than being the lowest, and its activation energy was the lowest rather than the highest. The low activation energy is consistent with the fact that there was no CTE or curing shrinkage mismatch between the two unidirectional laminae and, as a result, no interlaminar stress between the laminae. This low value supports the notion that the interlaminar stress is important in affecting the activation energy. The high contact resistivity for the unidirectional case can be explained in the following way. In the crossply samples, the pressure during curing forced the fibers of the two laminae to press on to one another and hence contact tightly. In the unidirectional sample, the fibers of one of the laminae just sank into the other lamina at the junction, so pressure helped relatively little in the contact between fibers of adjacent laminae. Moreover, in the crossply situation, every fiber at the lamina–lamina interface contacted many fibers of the other lamina, while, in the unidirectional situation, every fiber had little chance to contact the fibers of the other lamina. Therefore, the number of contact points between the two laminae was less for the unidirectional sample than the crossply samples. Figure 3 also shows a small irreversible decrease in the room temperature contact resistivity after a heating–cooling cycle. This is mainly due to the decrease in moisture content during heating, as shown by testing specimens having various moisture contents, which were attained by allowing the specimens to sit in air for different lengths of time. The irreversibility vanished when the temperature change was small (e.g., temperature changing from 20 to 100 °C). The larger the temperature change, the more significant was the irreversibility. The slight irreversibility is consistent with the fact that the activation energy obtained during cooling was slightly less than that obtained during heating (table 2). Table 2 also shows that the heating rate essentially did not affect the activation energy.

2.4. Conclusion for section 2

The interlaminar interface in carbon-fiber (continuous)–epoxy-matrix composites was studied by measuring the contact electrical resistivity of this interface.

The contact resistivity was found to decrease with increasing curing pressure and to be higher for unidirectional than crossply composites. This is because the extent of direct contact between fibers of adjacent laminae increases with increasing curing pressure and, at the same curing pressure, the fibers of adjacent laminae press on to one another much more strongly for crossply than unidirectional composites. The lower the contact resistivity, the greater the extent of direct contact between fibers of adjacent laminae.

The activation energy for electrical conduction in the through-thickness direction was found to increase with increasing curing pressure and to be lower for unidirectional than crossply composites. This is because the residual interlaminar stress increases with increasing fiber volume fraction, which increases with increasing curing pressure, and

the residual interlaminar stress is higher for crossply than unidirectional composites. The higher the activation energy, the greater the interlaminar stress.

3. Interlaminar interface as a moisture sensor

3.1. Introduction

Moisture is known to affect negatively numerous properties of polymers and their composites. This problem is of particular concern to advanced structural composites, since they are often used in demanding applications such as aircraft, helicopter rotor blades, fan blades and ocean platforms. Requirements on performance, durability and safety are strict for such applications.

Advanced structural composites are mainly polymer-matrix components containing continuous fibers such as carbon fibers, which are attractive for their high modulus, high strength, low density, and thermal conductivity. Among the polymer matrices used for carbon-fiber composites, epoxy (a thermoset) is most common.

Considerable attention has been given by numerous workers to address the effect of moisture on the mechanical behavior of polymer-matrix composites, as the mechanical behavior is relevant to the effectiveness for structural applications. In the case of carbon-fiber–epoxy-matrix composites, the properties which are dominated by the matrix or the fiber–matrix interface are degraded by moisture absorption, whereas the properties that are dominated by the fibers are essentially not affected [22]. In particular, the interfacial strength [23], the interlaminar tensile strength [24], the mode II critical strain-energy release rate [25], and the mode II interlaminar fracture toughness [26, 27] are degraded by moisture. The degradation is attributed to the weakening of the fiber–matrix bond [22, 28], the swelling action of the water [29], the softening of the matrix [22, 28], and the loss of shear strength of the matrix [27]. On the other hand, the curing residual stress is decreased by moisture [24] and the matrix can be plasticized by water [29], thereby increasing the fracture (delamination) toughness [29] or causing moisture to have little effect on the fracture properties [30] in some cases. The moisture effect is aggravated greatly by increasing the temperature [31–34], by using glass fiber in place of carbon fiber [35, 36], or by subjecting the composite to stress [37]. The composite material properties that are affected negatively by moisture include the stiffness [38, 39], the erosion resistance [40], the friction and wear properties [41], the creep compliance [42], the damping ratio [43], the maximum service temperature [44], and the resistance to curvature in the case of non-symmetric laminates [45]. The problem can be alleviated by surface treatment of the carbon fiber [46–48]. The moisture absorption proceeds by diffusion and the absorption is at least partially reversible [49].

In contrast to prior work [22–49], this section uses electrical resistivity measurement to investigate the effect of moisture on carbon-fiber–epoxy-matrix composites. The quantity measured is the contact electrical resistivity of the interlaminar interface (i.e., interface between adjacent laminae in a composite). Because the interlaminar interface is a common site of damage in composites, it makes sense to

Table 3. Carbon-fiber and epoxy-matrix properties (according to Cape Composites Inc., San Diego, CA).

Fortafil 555 continuous carbon fiber	
Diameter	6.2 μm
Density	1.8 g cm^{-3}
Tensile modulus	231 GPa
Tensile strength	3.80 GPa
Cape C2002 epoxy	
Processing temperature	121 $^{\circ}\text{C}$
Flexural modulus	99.9 GPa
Flexural strength	1.17 MPa
T_g	129 $^{\circ}\text{C}$
Density	1.15 g cm^{-3}

focus on this interface in studying the effect of moisture. The contact electrical resistivity of this interface is affected by the interfacial structure [50–54].

3.2. Experimental methods

Two laminae of unidirectional carbon-fiber–epoxy-matrix prepregs (provided by Cape Composites Inc., San Diego, CA) (table 3) in the form of strips crossing one another, with one strip on top of the other (figure 2(a)), were fabricated into a composite at the overlapping region (3.7 mm \times 3.7 mm) of the two laminae by applying pressure (from 0 to 1.2 MPa) and heat to the overlapping region (without a mold). Pressure and heat were provided to the junction as described in section 2.2. Each of the specimens was put between the two heating platens of the hot press and heated linearly up to 121 ± 2 $^{\circ}\text{C}$ at the rate of 2 $^{\circ}\text{C min}^{-1}$. Then it was cured at that temperature for 3 h and subsequently furnace cooled to room temperature.

Humidity variation was conducted after curing and subsequent cooling of the composite by using water (in a shallow dish) as the source of water vapor and desiccant (also in a shallow dish) to absorb the water vapor. The sample, a moisture sensor, and a hygrometer were all placed in a closed plastic box with the size of 20 inches (length) \times 15 inches (width) \times 7 inches (height). Vaseline was applied between the cover and the box to improve the seal. The procedure to vary the relative humidity is described below for one cycle of humidity variation. A dish of desiccant was placed in the box, and the box was closed with the cover. When the relative humidity had dropped below 10% RH, the box was opened, the desiccant was taken out, a dish of water was put in, and the box was closed. When the relative humidity had risen to above 90% RH, the box was opened, the dish of water was replaced with a dish of desiccant, and the box was closed. When the relative humidity dropped to 10% RH again, the humidity variation cycle was considered complete.

All the time, the contact electrical resistance was measured as described in section 2.2. The relative humidity was measured by the humidity sensor (model IH3605A, manufactured by Honeywell Microswitch) with the accuracy of $\pm 2.0\%$ RH, placed near the center of the sample. The sensor had a voltage input and a voltage output. The input was set to be 5 V, as provided by a DC power supply. Both the output voltage and the input voltage were measured by the Keithley 2001 multimeter. The relative humidity was calculated by a formula (provided by the manufacturer of the sensor) consisting of the output voltage, the input voltage and some constants.

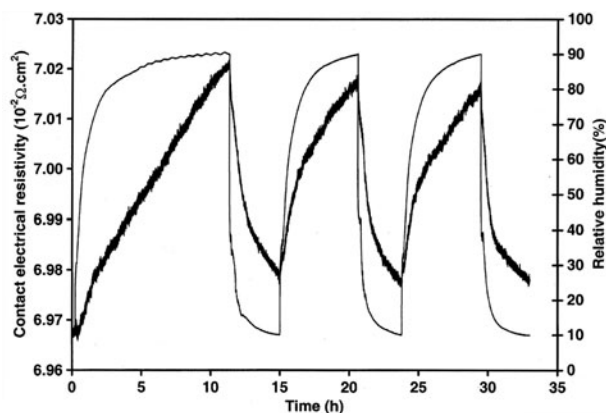


Figure 5. Variation of the contact electrical resistivity (thick curve) with time and of the relative humidity (thin curve) with time during humidity variation for composite made at a curing pressure of 0.63 MPa. (a) First cycle of humidity variation. (b) Second cycle of humidity variation.

The relative humidity was also monitored by a hygrometer with a digital output. The difference between the relative humidity indicated by the sensor and that indicated by the hygrometer was less than $\pm 2\%$ RH when the relative humidity was stable. When the relative humidity was changing, the humidity sensor reacted much faster than the hygrometer. So the sensor was used for relative humidity measurement in this work.

3.3. Results and discussion

Figure 5 shows the variation of the contact resistivity with time and of the relative humidity with time during cycling of the relative humidity for the composite made at a curing pressure of 0.21 MPa. The resistivity increased reversibly upon humidity increase. The reversibility was essentially complete after the first cycle of humidity variation. The behavior was similar for composites made at other curing pressures ranging from 0 to 1.2 MPa.

The observed trend is attributed to the distance between the fibers of adjacent laminae increasing as the epoxy matrix between the laminae expands during moisture uptake.

Moisture causes expansion of the epoxy matrix, as discussed above. On the other hand, an increase in temperature also causes expansion of the epoxy matrix, due to thermal expansion. In the study of the effect of temperature on the contact resistivity (section 2), we observed that an increase in temperature caused the resistivity to decrease, irrespective of the curing pressure. This suggests that the expansion resulting from moisture uptake is not the same as that resulting from heating. The relief of residual stress upon heating is significant, whether the curing pressure is high or low.

3.4. Conclusion for section 3

Moisture was found to have a reversible effect on the interlaminar interface of a continuous crossply carbon-fiber–epoxy-matrix composite. An increase in humidity increased the resistivity quite reversibly. The effect is attributed to the distance between fibers of adjacent laminae increasing as the epoxy matrix expanded upon moisture uptake. The effect is potentially useful for humidity sensing.

4. Interlaminar interface as a damage sensor

4.1. Introduction

Carbon-fiber-polymer-matrix composites are important materials for lightweight structures. However, the polymer matrix in these composites limits its high temperature resistance [55–58]. Moreover, the large mismatch in the coefficient of thermal expansion (CTE) between the polymer matrix and the carbon fibers causes thermal stress, which can cause cracks in the polymer. The cracking causes the modulus of the composite to decrease. As a consequence, the vibrations of the structure become more severe. This leads to more damage in a cumulative fashion. Thermal cycling makes the problem worse [59, 60]. Thermal cycling is encountered during infrared deicing of aircraft. During deicing, the temperature can reach 54 °C. Thermal cycling is also encountered during use of an aircraft, as ground and flight temperatures usually differ.

Although it is accepted in practice (based on experience) that infrared deicing below 66 °C does not cause appreciable degradation, the creep resistance is significantly reduced at 50 °C [61] and reported studies of thermal cycling involve temperatures of 120 °C or above [60]. Thus, thermal cycling studies at lower temperatures are needed.

This section is an investigation of the thermal damage of carbon-fiber-epoxy-matrix composites during thermal cycling between 18 °C and temperatures ranging from 23 to 200 °C. Due to the relatively low temperatures used for some of the testing, the extent of damage can be small. Therefore, the method of damage detection must be sensitive. Delamination or matrix cracking is a common form of damage in composites, in contrast to fiber fracture, which is a less common form of damage due to its association with severe damage. Delamination or matrix cracking can be detected by an increase in the contact electrical resistivity of the interface between laminae, since the damage decreases the number of contacts between fibers of adjacent laminae. An increase in the contact resistivity of the interlaminar interface leads to an increase in the volume electrical resistivity in the through-thickness direction. The volume resistivity has been previously used to indicate delamination during mechanical fatigue of carbon-fiber-epoxy-matrix composites [12], but the contact resistivity is a more direct indicator and is used in this work for monitoring damage. The non-destructive nature and high data acquisition rate of contact resistivity measurement allow the monitoring of the thermal damage in real time. Furthermore, the reversible decrease of the contact resistivity during heating within a thermal cycle allows temperature monitoring, while an increase in the contact resistivity during heating indicates damage. Hence, contact resistivity measurement provides information on the point in a temperature cycle at which damage occurs. In addition, it allows study of the mechanism behind the thermal damage.

Thermal fatigue is to be distinguished from mechanical fatigue, which is due to stress cycling and has received more attention [62–67]. The deformation during stress cycling causes temperature changes [66, 67]. However, due to the high thermal conductivity of carbon fibers, the resulting amplitude of temperature change in mechanical fatigue is small, typically below 1 °C. The amplitude of temperature change in thermal fatigue is much larger.

Thermal fatigue is conventionally studied by mechanical testing (usually destructive due to strength measurement) at room temperature after various numbers of cycles of temperature excursion [68–71]. Non-destructive mechanical testing (e.g., modulus measurement) at various temperatures during the temperature cycling is less common due to the greater complexity of the experimental set-up, but it is real-time monitoring and provides more precise information on the progress of thermal fatigue. Moreover, a specimen for mechanical testing (say by flexure) cannot be too small and a small specimen size is necessary for temperature variation at a reasonably high rate in order for thermal fatigue testing of the specimen to be completed within a reasonable length of time. Therefore, this work does not use mechanical testing for thermal fatigue monitoring, but rather uses electrical resistance measurement, which can be conducted on small specimens. The technique involves measuring the contact electrical resistivity of the interlaminar interface. Degradation of this interface causes this resistivity to increase.

The through-thickness resistance of a fiber composite consists of the volume resistance of each lamina in the through-thickness direction and the contact resistance of each interlaminar interface. The through-thickness resistance has been previously used to monitor in real time mechanical fatigue which causes delamination [12]. A change in the through-thickness resistance mainly reflects a change in the contact resistance of the interlaminar interface. The through-thickness resistance increases when delamination occurs. Thus, based on the through-thickness resistance, it was observed that delamination starts at 33% of the fatigue life. This section uses the contact resistance rather than the through-thickness resistance to indicate damage, since the contact resistance gives more direct information on the interlaminar interface.

By using contact electrical resistivity measurement, this section provides real-time monitoring of thermal fatigue of a carbon-fiber-polymer-matrix composite over a large number of temperature cycles. This monitoring entails that of both the damage and the temperature. Damage causes the resistivity to increase, whereas temperature increase causes the resistivity to decrease (section 2). Simultaneous monitoring of temperature and thermal damage during thermal fatigue is valuable, since it provides information on exactly which point of which temperature cycle at which damage occurs. Damage can occur at the highest temperature point, the lowest temperature point, or any other point of a temperature cycle. This is akin to the simultaneous monitoring of strain and mechanical damage during mechanical fatigue by through-thickness resistance measurement [62]. In contrast, the techniques such as acoustic emission can monitor damage, but cannot monitor temperature or strain.

A crossply configuration is used in this work for thermal fatigue monitoring, because the thermal stress and the sensitivity for temperature monitoring are higher for a crossply configuration than a unidirectional configuration (section 2). However, a unidirectional configuration could have been used instead.

4.2. Experimental methods

The materials and sample preparation were the same as those in section 3.2, except that the applied pressure was 0.33 MPa during composite fabrication.

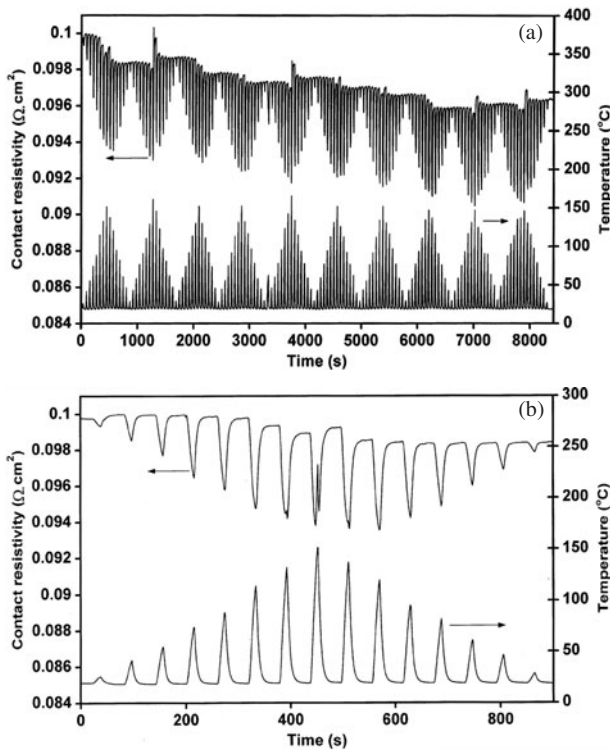


Figure 6. Variation of the contact electrical resistivity with time and of the temperature with time during thermal cycling.

Thermal cycling was conducted after curing and subsequent cooling of the composite by using a small resistance heater and using compressed air and a copper tubing with flowing water for cooling. All the time, the contact electrical resistance and the temperature of the sample were measured, as described in section 2.2.

4.3. Results and discussion

Figure 6 shows the variation of the contact resistivity with temperature during thermal cycling. The temperature was repeatedly increased to various levels. A group of cycles in which the temperature amplitude increased cycle by cycle and then decreased cycle by cycle back to the initial low temperature amplitude is hereby referred to as a group. Figure 6(a) shows the results of the first ten groups, while figure 6(b) shows the first group only. The contact resistivity decreased upon heating in every cycle of every group. At the highest temperature (150 °C) of a group, a spike of resistivity increase occurred, as shown in figure 6(b). This spike was observed similarly in other groups. It is attributed to damage at the interlaminar interface. In addition, the baseline resistivity (i.e., the top envelope) gradually and irreversibly shifted downward as cycling progressed, as shown in figure 6(a). The baseline decrease is probably due to matrix damage within a lamina and the resulting decrease in modulus and hence decrease in residual stress; it is not due to thermal fatigue, since the damage was most significant in the early cycles and incremental damage diminished upon thermal cycling.

Figure 7 shows similar results for a case of more severe damage occurring at the highest temperature (170 °C) of a group. The damage resulted in a large spike of resistivity

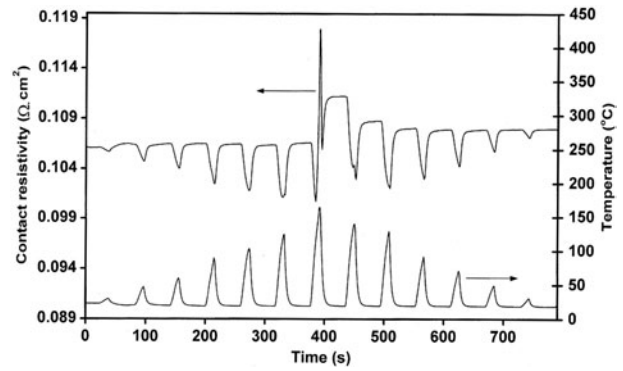


Figure 7. Variation of the contact electrical resistivity with time and of the temperature with time during thermal cycling for thermoset-matrix composite.

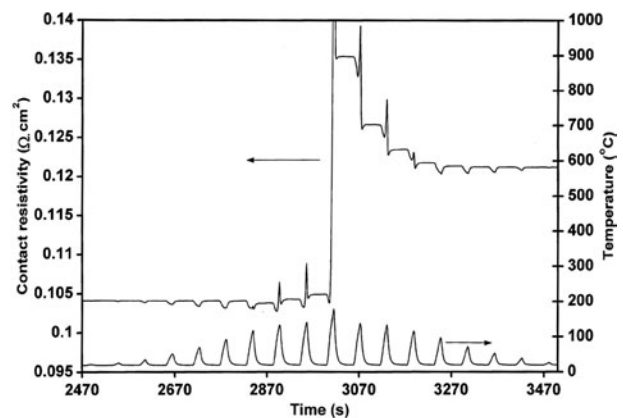


Figure 8. Variation of the contact electrical resistivity with time and of the temperature with time during thermal cycling for thermoset-matrix composite.

increase at the highest temperature, in addition to a partially reversible upward shift of the baseline resistivity immediately after the spike. The extent of upward shift decreased rapidly from cycle to cycle during the two cycles immediately following the spike.

Figure 8 shows similar results for a case of even more severe damage. A spike of resistivity increase occurred at the peak temperature of a cycle for quite a few cycles in a group (not just for the cycle with the highest peak temperature), such that the spike became larger as the peak temperature increased. The lowest peak temperature at which a spike was observed was 110 °C (below the composite processing temperature of 121 °C). Furthermore, a partially reversible upward shift of the baseline resistivity occurred immediately after the spike at the highest temperature (200 °C) of the group. This shift is more severe than that in figure 7.

The greater the damage (related to interlaminar interface damage), the more severe is the spike or contact resistivity increase and the greater is the partially reversible baseline resistivity increase following the spike (figures 6–8). As expected, the higher the temperature, the greater is the extent of damage. In addition, minor damage (probably related to matrix damage) occurred gradually as cycling progressed, leading to a gradual and irreversible decrease of the baseline resistivity.

The spike of contact resistivity increase is particularly sensitive to damage, even to slight damage occurring at 110 °C.

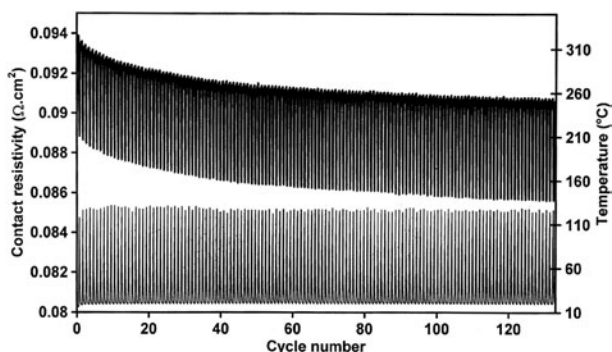


Figure 9. Variation of the contact electrical resistivity (thick curve) with cycle number and of the temperature (thin curve) with cycle number during the first 133 thermal cycles for thermoset-matrix composite.

The size of the spike indicates the extent of damage. The time of the spike is the time of the damage occurrence. The partially reversible baseline resistivity increase following a relatively large spike is an additional indicator, which is sensitive to only relatively large extents of damage. Both the spike and the partially reversible baseline resistivity increase following the spike are valuable for monitoring damage in real time. On the other hand, the gradual and irreversible baseline resistivity decrease that occurs as cycling progresses is useful for condition monitoring, whether in real time or not. It is particularly valuable for monitoring minor damage, which is not accompanied by a partially reversible baseline resistivity increase following a spike. As shown in figure 6(b), the gradual and irreversible baseline decrease starts to occur at lower temperatures than the spike.

Figure 9 shows the variation of the contact resistivity with temperature during initial thermal cycling. In each thermal cycle, the contact resistivity decreased with increasing temperature and increased with decreasing temperature, because increasing temperature increased the probability of electron jumping from one lamina to the other (section 2). It can also be noticed that the baseline of the contact resistivity decreased and gradually leveled off with increasing thermal cycle number. There are two possible reasons for the decrease. One reason is that the moisture content decreased with increasing thermal cycle number, due to the heating driving out moisture from the epoxy matrix. (Although the moisture could partly come back in the cooling part of each cycle, the moisture absorption was much slower than the moisture desorption during heating.) Moisture made the epoxy expand. Therefore, the lower the moisture content, the higher the density of the epoxy, the higher the fiber volume fraction, the greater the number of fiber contacts between the two laminae, and the lower the contact resistivity. The other possible reason is that the thermal cycling damaged the epoxy matrix, thereby decreasing the modulus of the laminae, lowering the thermal stress, and decreasing the contact resistivity. This damage is not really due to thermal fatigue, since the damage was most significant in the first cycle and incremental damage diminished upon thermal cycling.

Figure 10 shows that a small spike of contact resistivity increase occurred at the maximum temperature of a cycle from cycle no 13 481 onward. The increase was partly reversible and is attributed to thermal fatigue damage of the interlaminar

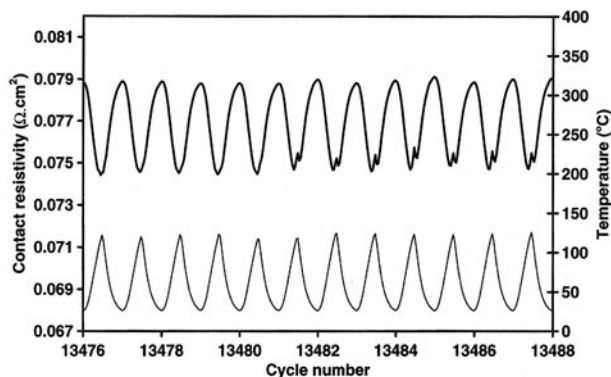


Figure 10. Variation of the contact electrical resistivity (thick curve) with cycle number and of the temperature (thin curve) with cycle number from cycle no 13 476 to cycle no 13 487 for thermoset-matrix composite. The spike started to appear at cycle no 13 481 and continued thereafter.

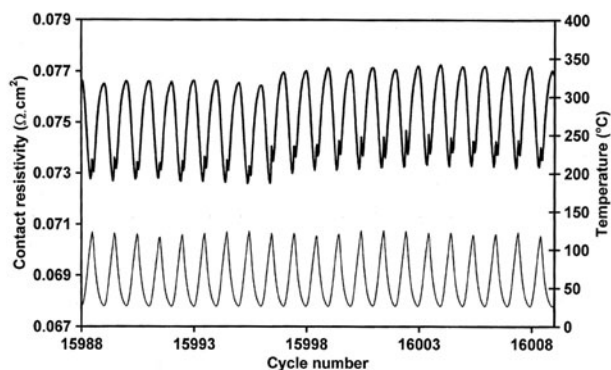


Figure 11. Variation of the contact electrical resistivity (thick curve) with cycle number and of the temperature (thin curve) with cycle number from cycle no 15 988 to cycle no 16 008 for thermoset-matrix composite. An abrupt increase in the baseline of the contact electrical resistivity occurred at cycle no 15 996.

interface. The damage may be a form of delamination and increased the contact resistivity.

Figure 11 shows another result of thermal fatigue, which occurred later in the fatigue life. It involved an abrupt increase of the contact resistivity baseline. The abrupt increase, which occurred more than once, also indicates damage of the interlaminar interface—perhaps more serious damage than that indicated by the spikes, which occurred earlier in the fatigue life.

4.4. Conclusion for section 4

The contact electrical resistivity of the interlaminar interface was used to monitor thermal damage in a continuous carbon-fiber–epoxy-matrix composite in real time during thermal cycling. Thermal damage in the form of damage to the interlaminar interface caused a spike of contact resistivity increase at the time of damage occurrence and, in the case of more extensive damage, also a partially reversible resistivity baseline increase following the spike. Thermal damage, probably in the form of matrix damage in the laminae, caused a gradual and irreversible decrease of the resistivity baseline. The lowest temperature at which thermal damage was observed was 110°C (below the composite processing temperature).

The higher the temperature, the more extensive was the damage, and the more severe were the effects on the contact resistivity.

Thermal fatigue in a continuous carbon-fiber–epoxy-matrix composite was monitored in real time during thermal cycling between 28 and 118 °C by measurement of the contact electrical resistivity of the interlaminar interface. Simultaneous to the monitoring of the damage was the monitoring of the temperature by the same resistivity measurement, as the resistivity decreased reversibly upon heating in each thermal cycle, due to the energy barrier for electron jumping from one lamina to the other. The initial stage of damage occurred primarily during the first 100 thermal cycles, and was associated with decrease of the resistivity baseline, probably due to moisture desorption and/or matrix modulus decrease. The second stage of damage involved thermal fatigue damage in the form of interlaminar interface degradation (probably delamination), which was associated with a spike of resistivity increase at the maximum temperature of a thermal cycle. The third stage of damage involved thermal fatigue damage, also in the form of interlaminar interface degradation, which was associated with abrupt increases of the resistivity baseline.

5. Interlaminar interface as a stress sensor

5.1. Introduction

Strain/stress sensing has been attained in continuous carbon-fiber–polymer-matrix composites by using the piezoresistive behavior of the bulk composite [1–17]. This behavior involves the volume electrical resistivity of the composite in the longitudinal (fiber) direction decreasing reversibly upon longitudinal tension and that in the through-thickness direction increasing reversibly upon longitudinal tension. The use of the volume resistivity distribution to determine a two-dimensional strain distribution is tedious, as it requires the application of a two-dimensional array of electrical contacts.

In this section, the interlaminar interface is used as a piezoresistive stress (compressive) sensor. By using two crossply laminae, a two-dimensional array of strain sensors and an x – y grid of electrical interconnections are obtained (figure 1), thus allowing compressive stress distribution sensing, in which the composite is utilized as both sensors and electrical interconnections.

Thermoplastics are in general more ductile than thermosets. Thus, the piezoresistive effect associated with the interlaminar interface is expected to differ between thermoplastic-matrix and thermoset-matrix composites. This work addresses the piezoresistive effect in both types of composite. Epoxy is the thermoset matrix used in this study and nylon-6 polyamide is the thermoplastic matrix used in this study, as these matrices are among the most common for fiber structural composites.

5.2. Experimental methods

Epoxy-matrix materials and associated sample preparation were as described in section 3.2, except that the overlapping regions of the two crossply laminae were of size 6 mm × 6 mm

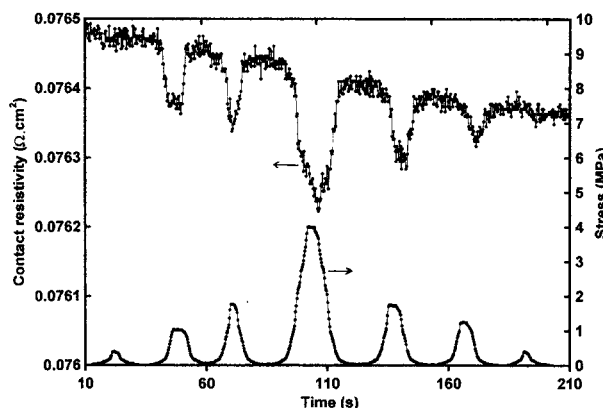


Figure 12. Variation of the contact electrical resistivity with time and of the stress with time during stress cycling of an epoxy-matrix composite at different stress amplitudes up to 4 MPa.

and the applied pressure during composite fabrication was 0.43 MPa.

The thermoplastic polymer was nylon-6 (PA) in the form of unidirectional carbon-fiber prepregs supplied by Quadrax Corp. (Portsmouth, RI; QNC 4162). The fibers were 34–700 from Grafil, Inc. (Sacramento, CA). The fiber diameter was 6.9 μm . The fiber weight fraction in the prepreg was 62%. The glass transition temperature (T_g) was 40–60 °C and the melting temperature (T_m) was 220 °C for the nylon-6 matrix. The prepreg thickness was 250 μm . The prepreg was used as received. Prepreg strips 6 mm in width were placed on one another at an angle of 90° in a cross-shaped steel mold cavity lined with a PTFE film for electrical insulation, so that the overlap area was 6 mm × 6 mm, as shown in figure 2(a). During formation of the interlaminar interface at the overlap area, the temperature was raised from 20 to 260 °C ($T_m = 220$ °C) at a heating rate of 10 °C min^{-1} and a pressure of 2.0 MPa and then held at temperature and pressure for 30 min. After that, the specimen was furnace cooled to room temperature. Throughout the heating and cooling, pressure (2 MPa, as provided by steel plates of known weights) was applied through a 3 cm long cross-shaped steel plate, which was electrically insulated from the prepreg strips by a PTFE film.

A dynamic compressive stress (up to a stress amplitude of 216 MPa) was applied on the overlapping region (figure 2(a)) by using a screw-action mechanical testing system (Sintech 2/D, MTS Systems Corp., Eden Prairie, MN). Simultaneously, the contact electrical resistance was measured, as described in section 2.2.

5.3. Results and discussion

5.3.1. Epoxy-matrix composite. Figure 12 shows the variation of the contact resistivity with stress during compressive stress cycling of the epoxy-matrix composite to various maximum stresses up to 4 MPa. The contact resistivity decreased reversibly upon loading, due to the increased contact between fibers of adjacent laminae. The resistivity decrease was partially reversible. The greater the stress, the more the contact resistivity decreased. Although figure 12 shows results at stress amplitudes up to 4 MPa, similar results were obtained up to 27 MPa.

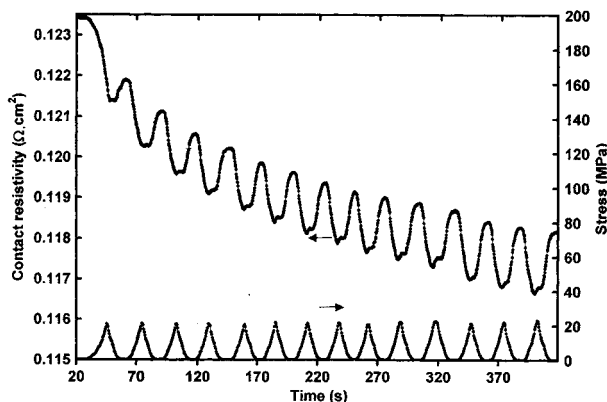


Figure 13. Variation of the contact resistivity with time and of the stress with time during stress cycling at a constant stress amplitude of 27 MPa for a thermoset-matrix composite.

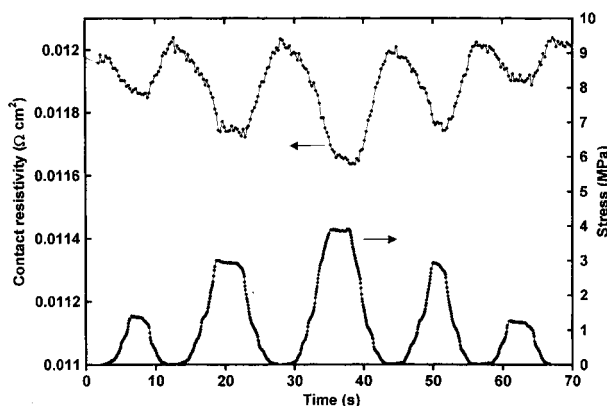


Figure 14. Variation of the contact electrical resistivity with time and of the stress with time during stress cycling of a nylon-matrix composite at different stress amplitudes up to 4 MPa.

The upper envelope of the resistivity variation in figure 12 decreased gradually cycle by cycle. This means that the resistivity decrease upon loading was not totally reversible. The partial irreversibility means that the increase in the extent of contact between fibers of adjacent laminae upon loading is not completely reversible. It is due to plastic deformation and/or very minor damage of the interlaminar interface.

Stress cycling at a fixed stress amplitude of 27 MPa for 14 cycles (figure 13) showed that both the upper and lower envelopes of the resistivity decreased irreversibly and gradually leveled off as cycling progressed, while the reversible effect within a cycle was essentially not affected. The irreversible effect is due to minor damage of the interlaminar interface. The effect was much more severe than that at a lower stress amplitude (figure 12). It was most significant in the first two cycles and subsequent incremental effect diminished as cycling progressed. A possible damage mechanism is matrix damage which led to an irreversible increase in the extent of contact between fibers of adjacent laminae. The effect could not have been due to plastic deformation, as plastic deformation would have been much more severe in the thermoplastic case (next section) but the phenomenon was not observed in the thermoplastic case.

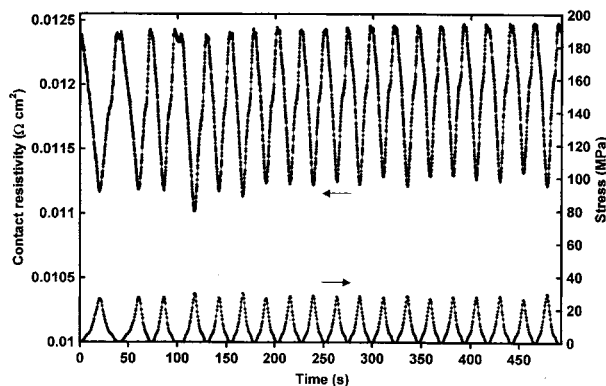


Figure 15. Variation of the contact electrical resistivity with time and of the stress with time during stress cycling at a constant stress amplitude of 27 MPa for a thermoplastic-matrix composite.

5.3.2. Thermoplastic-matrix composite. Figure 14 shows results akin to figure 12, but for the thermoplastic-matrix composite. The resistivity decreased upon compression, such that the effect was totally reversible, in contrast to the partially reversible behavior of the epoxy-matrix composite. The fractional change in resistivity per unit stress was 8×10^{-4} and $8 \times 10^{-3} \text{ MPa}^{-1}$ for epoxy and nylon-6 composites respectively, as measured at a stress amplitude of 4 MPa. This means that the piezoresistive effect was much larger for thermoplastic- than thermoset-matrix composites.

Figure 15 shows results akin to figure 13, but for the thermoplastic-matrix composite. The stress amplitude was 27 MPa. The resistivity decreased reversibly in every cycle. The upper envelope of the resistivity variation shifted upward very slightly and gradually as cycling progressed. The shift is negligible compared to that in the epoxy case (figure 13). It is attributed to very minor damage of the interlaminar interface. A possible damage mechanism is the formation of defects that led to a decrease in the extent of contact between fibers of adjacent laminae.

Results similar to figure 15 were obtained up to a stress amplitude of 216 MPa. Even at a stress amplitude of 216 MPa, the resistivity decreased reversibly in every cycle and the upshift of the envelope of resistivity variation was almost negligible.

5.3.3. General discussion. The interlaminar interface of a crossply carbon-fiber-polymer-matrix composite functions as a piezoresistive stress sensor. The sensitivity is much higher and the repeatability is much better for a thermoplastic-matrix composite than a thermoset-matrix composite, due to the higher elastic limit of a thermoplastic compared to a thermoset. For the thermoplastic case, the stress sensitivity and repeatability are good up to a compressive stress of 216 MPa. (Higher stress levels were not used.) For both matrices, the piezoresistive effect originates from the increase in the degree of contact between fibers of adjacent laminae as the compressive stress increases.

The interlaminar interface of a unidirectional composite is probably piezoresistive also. However, the crossply configuration is practically attractive, as it provides a two-dimensional array of piezoresistive sensors for stress

distribution sensing, in addition to providing an x - y grid of electrical interconnections.

The reversible phenomenon reported is useful for stress sensing, but cannot be used for strain sensing. This is because correlation of the resistivity with strain at the interlaminar interface is experimentally difficult.

5.4. Conclusion for section 5

The interlaminar interface of a carbon-fiber-polymer-matrix composite is a piezoresistive stress sensor, as the contact electrical resistivity of the interface decreases with compressive stress (up to 216 MPa) in the direction perpendicular to the interface. The phenomenon is due to an increase in the number of contacts between fibers of adjacent laminae. The piezoresistive effect was much larger and much more repeatable for a thermoplastic-matrix composite than a thermoset-matrix composite. It was essentially reversible for a thermoplastic-matrix composite, but was partially reversible for a thermoset-matrix composite. The partial irreversibility is due to minor damage of the thermoset interlaminar interface, particularly during the first two stress cycles.

6. Interlaminar interface as a thermocouple junction

6.1. Introduction

Thermoelectric phenomena involve the transfer of energy between electric power and thermal gradients. They are widely used for cooling and heating, including air conditioning, refrigeration, thermal management, and the generation of electrical power from waste heat.

A thermocouple is a thermoelectric thermometric device that involves a junction between two dissimilar materials. The voltage between the two dissimilar materials at the ends away from the junction relates to the temperature difference between the junction and these ends. The physics lies in the Seebeck effect, i.e., the movement of the mobile charge carriers from the hot point to the cold point of each dissimilar material and the consequent voltage difference between the hot and cold points of each dissimilar material.

The dissimilar materials used for thermocouples are conventionally metals. This section provides thermocouples in the form of continuous carbon-fiber-polymer-matrix composites. Carbon fibers are used because of their electrical and thermal conductivity. The interlaminar interface (i.e., interface between adjacent laminae in a composite) serves as the junction in the thermocouple. The dissimilar materials are laminae with different types of carbon fiber (fibers that differ in carrier type and/or concentration).

The advantages of fiber composite thermocouples compared to conventional thermocouples are low cost, mechanical ruggedness, processability into various shapes and sizes, and that the thermocouple is itself the structure. The last advantage means that the structure is itself thermocouples, thus making the structure able to monitor its temperature without the need for embedded or attached devices. This translates to low cost, high durability, large sensing volume, and absence of mechanical property degradation (which occurs in the case of embedded sensors).

The Seebeck effect involving a single type of material rather than dissimilar materials has been reported in carbon fibers (no matrix) [72–74] and in carbon-fiber composites [75, 76]. The use of dissimilar materials allows the voltage measurement to be made at only one end (say the end at room temperature) of the dissimilar materials, thus making thermocouples convenient to use. Furthermore, appropriate selection of the dissimilar materials can make the change in measured voltage per unit rise in temperature (i.e., thermocouple sensitivity) larger than the Seebeck coefficient of a single type of material.

Carbon fibers can be n-type or p-type even without intercalation. Intercalation greatly increases the carrier concentration, thus making the fibers strongly n-type or strongly p-type, depending on whether the intercalate is an electron donor or an electron acceptor. There had been a study of the thermopower of intercalated carbon fibers [74]. This section shows that thermocouples involving n-type and p-type forms of carbon fibers are particularly sensitive.

One of the drawbacks of intercalated graphite is the instability over time, either due to intercalate desorption or reaction with environmental species. For the case of bromine (acceptor) as the intercalate, the instability due to desorption can be overcome by the use of a residue compound, i.e., a compound that has undergone desorption as much as possible so that the remaining intercalate is strongly held, thereby making the compound stable. The stability of bromine intercalated carbon fibers has been previously demonstrated [77–79]. For the case of an alkali metal such as sodium (donor) as the intercalate, the instability due to reactivity with moisture can be overcome by the use of an alkali metal hydroxide (with the alkali metal ions in excess) as the intercalate [80]. Therefore, this section uses bromine as the acceptor intercalate and sodium hydroxide (with Na^+ ions in excess) as the donor intercalate.

Although considerable attention has been given to intercalated carbon fibers, little attention has been given to composites that involve these fibers [81–83]. Previous work on these composites has been focused on the electrical conductivity, due to the relevance to electromagnetic interference shielding and other applications. In contrast to previous work, this section addresses the thermoelectric behavior of the composites, particularly composites involving dissimilar carbon fibers that meet at a junction to form a thermocouple.

6.2. Experimental methods

The carbon fibers used were Thornel P-25, P-100, and P-120 2K pitch based fibers (Amoco Performance Products, Alpharetta, GA) and T-300 PAN based fibers (in the form of 976 epoxy unidirectional fiber prepregs, Hy-E 1076E, ICI Fiberite, Tempe, AZ).

Intercalation was carried out only for P-100 and P-120 fibers, due to their relatively high crystallinity. Bromine intercalation involved exposure to bromine vapor in air at room temperature for 10 days, followed by desorption in a fume hood at room temperature for several months. Sodium hydroxide intercalation involved immersion of the fibers in a liquid solution of NaOH and molten sodium contained in a nickel crucible. The atomic ratio of Na to NaOH was

Table 4. Seebeck coefficient ($\mu\text{V } ^\circ\text{C}^{-1}$) and absolute thermoelectric power ($\mu\text{V } ^\circ\text{C}^{-1}$) of carbon fibers and thermocouple sensitivity ($\mu\text{V } ^\circ\text{C}^{-1}$) of epoxy-matrix composite junctions. All junctions are unidirectional unless specified as crossply. The temperature range is 20–110 $^\circ\text{C}$.

	Seebeck coefficient with copper as the reference ($\mu\text{V } ^\circ\text{C}^{-1}$)	Absolute thermoelectric power ($\mu\text{V } ^\circ\text{C}^{-1}$)	Thermocouple sensitivity ($\mu\text{V } ^\circ\text{C}^{-1}$)
P-25 ^a	+0.8	+3.1	
T-300 ^a	−5.0	−2.7	
P-25 ^a + T-300 ^a			+5.5
P-25 + T-300 ^a (crossply)			+5.4
P-100 ^a	−1.7	+0.6	
P-120 ^a	−3.2	−0.9	
P-100 (Na)	−48	−46	
P-100 (Br ₂)	+43	+45	
P-100 (Br ₂) + P-100 (Na)			+82
P-120 (Na)	−42	−40	
P-120 (Br ₂)	+38	+40	
P-120 (Br ₂) + P-120 (Na)			+74

^a Pristine (i.e., not intercalated).

1:100. The procedure is described below. The crucible was placed in a small furnace, which was purged with argon gas. After the furnace had reached 350 $^\circ\text{C}$, sodium metal was added to the molten NaOH in the crucible. Then the fibers (protected by a nickel spring) were immersed in the liquid solution. The furnace was covered and the temperature of 350 $^\circ\text{C}$ was maintained for 4 h. After that, the fibers were removed and allowed to cool. Then the fibers (still protected by a nickel spring) were washed by flowing water for 12 h in order to remove the NaOH on the fiber surface. After this, the fibers were dried in a vacuum oven.

Thermocouple junctions were epoxy-matrix composite interlaminar interfaces. In this study, a junction was formed by allowing two laminae to overlap partially and then curing the stack under heat and pressure, as required for the curing of the epoxy matrix. The overlap region served as the junction; the remaining regions served as thermocouple wires. Those junctions involving T-300 fibers used the epoxy in the prepreg as the bonding agent for the junction. Those not involving T-300 fibers used epoxy resin 9405 and curing agent 9470 from Shell Chemical Co. (Houston, TX) as the epoxy matrix as well as bonding agent. Curing of the epoxy in the T-300 prepreg was conducted by heating in a hydraulic hot press at a rate of 2.5 $^\circ\text{C min}^{-1}$ and then maintaining the temperature for 2 h. The curing temperature was 175 $^\circ\text{C}$ for the epoxy in the T-300 prepreps and was 150 $^\circ\text{C}$ for the other epoxy. The curing pressure was 18 MPa for unidirectional junctions (i.e., the fibers in the two laminae oriented in the same direction) and 16 MPa for crossply junctions (i.e., the fibers in the two laminae oriented at 90 $^\circ$) involving the epoxy in the T-300 prepreps. For junctions involving the other epoxy, the curing pressure was 0.02 MPa.

Thermopower measurement was performed on the fibers (P-25, P-100 and P-120 fiber bundles without matrix, and T-300 prepreg with epoxy matrix) and on the epoxy-matrix composite junctions involving dissimilar fibers. The measurement in the former case involved attaching the two ends of a fiber bundle or prepreg to copper foils using a silver epoxy conductive adhesive, maintaining one copper foil at a controlled high temperature (up to 200 $^\circ\text{C}$) by using a furnace, and maintaining the other copper foil at a temperature near

room temperature. A copper wire was soldered at its end to each of the two copper foils. The copper wires were fed to a Keithley 2001 multimeter for measuring the voltage. T-type thermocouples were used for measuring the temperatures of the hot and cold ends. Voltage and temperature measurements were conducted simultaneously using the multimeter. The voltage difference (hot minus cold) divided by the temperature difference (hot minus cold) yielded the Seebeck coefficient with copper as the reference, since the copper wires at the two ends of a sample were at different temperatures. This Seebeck coefficient plus the absolute thermoelectric power of copper (+2.34 $\mu\text{V } ^\circ\text{C}^{-1}$) [9] is the absolute thermoelectric power of the composite. The thermopower measurement in the latter case involved the same configuration, except that the junction was at the hot point and the two ends of the sample away from the junction were attached using silver epoxy onto two copper foils, which were both at a temperature near room temperature.

In the case of pristine P-25 fibers without matrix, thermopower measurement was also made using fixed temperatures at the hot (100 $^\circ\text{C}$, boiling water) and cold (0 $^\circ\text{C}$, ice water) points and using four methods of attaching the sample ends to the copper foils (namely silver epoxy, silver paint, solder and brass clips). Results (Seebeck coefficient) obtained using these variations in methods are consistent with that obtained using the method described in the last paragraph, thus confirming the validity of the method used in this section.

In the case of the junction between pristine P-25 and pristine T-300 fibers in either unidirectional or crossply configuration, thermopower measurement was performed during the curing heating cycle as well as during subsequent heating and cooling.

6.3. Results and discussion

Table 4 shows the Seebeck coefficient and the absolute thermoelectric power of carbon fibers and the thermocouple sensitivity of epoxy-matrix composite junctions. A positive value of the absolute thermoelectric power indicates p-type behavior; a negative value indicates n-type behavior. Pristine P-25 is slightly p-type; pristine T-300 is slightly n-type. A junction comprising pristine P-25 and pristine T-300 has a positive thermocouple sensitivity that is close to

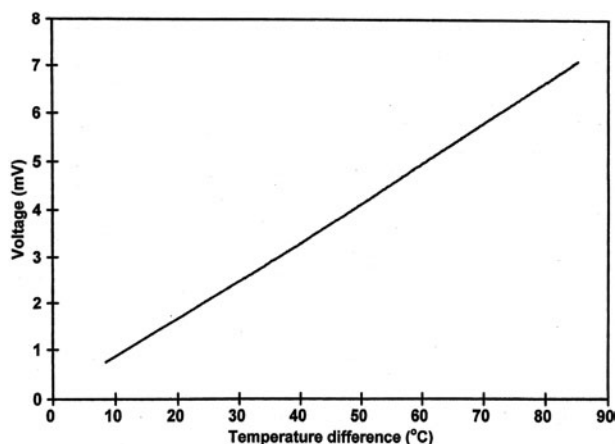


Figure 16. Variation of the measured voltage with the temperature difference between hot and cold points for the epoxy-matrix composite junction comprising bromine intercalated P-100 and sodium intercalated P-100.

the difference of the Seebeck coefficients (or the absolute thermoelectric powers) of T-300 and P-25, whether the junction is unidirectional or crossply. Pristine P-100 and pristine P-120 are both essentially neutral (i.e., neither n-type nor p-type). Intercalation with sodium causes P-100 and P-120 to become strongly n-type. Intercalation with bromine causes P-100 and P-120 to become strongly p-type. A junction comprising bromine intercalated P-100 and sodium intercalated P-100 has a positive thermocouple sensitivity that is close to the sum of the magnitudes of the absolute thermoelectric powers of the bromine intercalated P-100 and the sodium intercalated P-100. Similarly, a junction comprising bromine intercalated P-120 and sodium intercalated P-120 has a positive thermocouple sensitivity that is close to the sum of the magnitudes of the absolute thermoelectric powers of the bromine intercalated P-120 and the sodium intercalated P-120. Figure 16 shows the linear relationship of the measured voltage with the temperature difference between hot and cold points for the junction comprising bromine intercalated P-100 and sodium intercalated P-100.

A junction comprising n-type and p-type partners has a thermocouple sensitivity that is close to the sum of the magnitudes of the absolute thermoelectric powers of the two partners. This is because the electrons in the n-type partner as well as the holes in the p-type partner move away from the hot point toward the corresponding cold point. As a result, the overall effect on the voltage difference between the two cold ends is additive.

By using junctions comprising strongly n-type and strongly p-type partners, a thermocouple sensitivity as high as $+82 \mu\text{V } ^\circ\text{C}^{-1}$ was attained. Semiconductors are known to exhibit much higher values of the Seebeck coefficient than metals, but the need to have thermocouples in the form of long wires makes metals the main materials for thermocouples. Intercalated carbon fibers exhibit much higher values of the Seebeck coefficient than metals. Yet, unlike semiconductors, their fiber form and fiber composite form make them convenient for practical use as thermocouples.

The Seebeck coefficient of HNO_3 intercalated CVD carbon fibers is $15 \mu\text{V } ^\circ\text{C}^{-1}$ at 300 K [74]. Extrapolation of

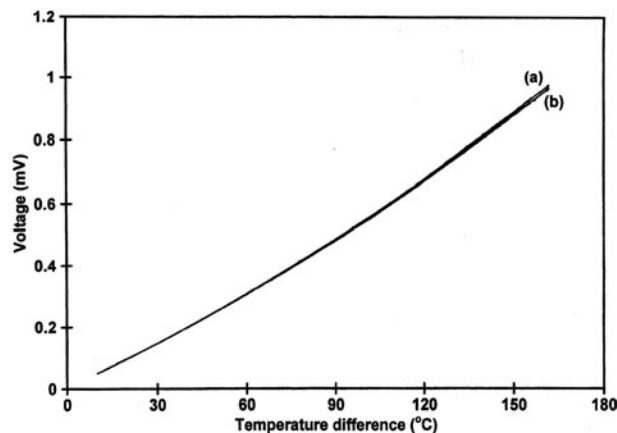


Figure 17. Variation of the measured voltage with the temperature difference between hot and cold points for the epoxy-matrix composite junction comprising pristine P-25 and pristine T-300, as obtained in the curing heating cycle. (a) Unidirectional configuration, (b) crossply configuration.

the data of [81] to 500 K gave a value of less than $20 \mu\text{V } ^\circ\text{C}^{-1}$. The values obtained in this work for intercalated fibers are considerably higher in magnitude.

Figure 17 shows the relationship between the measured voltage and the temperature difference between hot and cold points for the junction comprising pristine P-25 and pristine T-300, as obtained during the curing heating cycle. Even though the junction is essentially not cured during heating in the curing cycle and is already cured during cooling in the curing cycle, the curves during heating and cooling overlap. This means that the thermocouple sensitivity is independent of the nature of the interface. The curves for unidirectional and crossply configurations essentially overlap. The results obtained during subsequent heating and cooling are essentially the same as those in figure 17. The curves in figure 17 deviate positively from linearity, in contrast to the linearity in figure 16. A positive deviation from linearity is quite common among commercial thermocouples, such as T-type thermocouples.

That the thermocouple sensitivity of the carbon-fiber epoxy-matrix composite junctions is independent of the extent of curing and is the same for unidirectional and crossply junctions (table 4 and figure 17) is consistent with the fact that the thermocouple effect hinges on the difference in the bulk properties of the two partners, and is not an interfacial phenomenon. This behavior means that the interlaminar interfaces in a fibrous composite serve as thermocouple junctions in the same way, irrespective of the lay-up configuration of the dissimilar fibers in the laminate. As a structural composite typically has fibers in multiple directions, this behavior facilitates the use of a structural composite as a thermocouple array.

It is important to note that the thermocouple junctions do not require any bonding agent other than the epoxy, which serves as the matrix of the composite and does not serve as an electrical contact medium (since it is not conductive). In spite of the presence of the epoxy matrix in the junction area, direct contact occurs between a fraction of the fibers of a lamina and a fraction of the fibers of the other lamina, thus resulting in a conduction path in the direction perpendicular to the junction. This conduction path is indicated by direct measurement of the

electrical resistance of the junction (section 2) and enables an electrical contact to be made across the junction. The use of silver paint as an additional bonding agent did not give a better result, as we found experimentally. That the bonding agent did not affect the result is also consistent with the fact that the thermocouple effect is not an interfacial phenomenon. That an additional bonding agent is not necessary facilitates the use of a structural composite as a thermocouple array, as a typical structural composite does not have any extra bonding agent at the interlaminar interface.

The thermocouple effect can be used for converting thermal energy to electrical energy. To make the voltage generated of practical significance, a large number of thermocouples can be connected in series. In other words, the lamina configuration in the composite can be designed so as to provide a large number of thermocouples that are connected in series. Hence, the structural composite is an electric power generator, which may be useful for providing some of the electric power needed by aircraft made with composites.

6.4. Conclusion for section 6

Thermocouples made from n-type carbon fibers (e.g., sodium intercalated P-100 fibers) and p-type carbon fibers (e.g., bromine intercalated P-100 fibers) in the form of epoxy-matrix composites, using the interlaminar interface as the thermocouple junction, were found to exhibit thermocouple sensitivity up to $82 \mu\text{V } ^\circ\text{C}^{-1}$ —close to the sum of the magnitudes of the Seebeck coefficients of the two partners of the thermocouple. Bromine intercalation changed the Seebeck coefficient (with copper as the reference) of P-100 fibers from $+0.6$ to $+45 \mu\text{V } ^\circ\text{C}^{-1}$. Sodium intercalation changed it from $+0.6$ to $-46 \mu\text{V } ^\circ\text{C}^{-1}$. Similarly large effects were observed for intercalated P-120 fibers. Pristine fibers gave similar junctions, but with a much smaller value of the thermocouple sensitivity. The thermocouple sensitivity was the same for unidirectional and crossply junctions.

7. Interlaminar interface array for spatial distribution sensing

7.1. Introduction

Sections 2–6 describe the use of the interlaminar interface for self-sensing temperature, moisture, damage, and stress. As shown in figure 1, two crossply laminae provide a two-dimensional array of interlaminar interfaces. The use of this array for temperature distribution sensing is demonstrated in this section for the case of the interlaminar interface serving as a thermistor (section 2) and for the case of the interface serving as a thermocouple junction (section 6). In either case, the fiber groups that make contact at the interface also serve as electrical leads, thereby providing an x – y grid of electrical interconnections. Not all the groups need to serve as leads, because the spatial resolution of the detection does not need to be excessive.

The top two fiber layers of a composite structure capable of sensing should be crossply (figure 1). The layers below can be in other lay-up configurations. The fibers in the top two layers should be longer than those in the other layers in order to facilitate electrical connection.

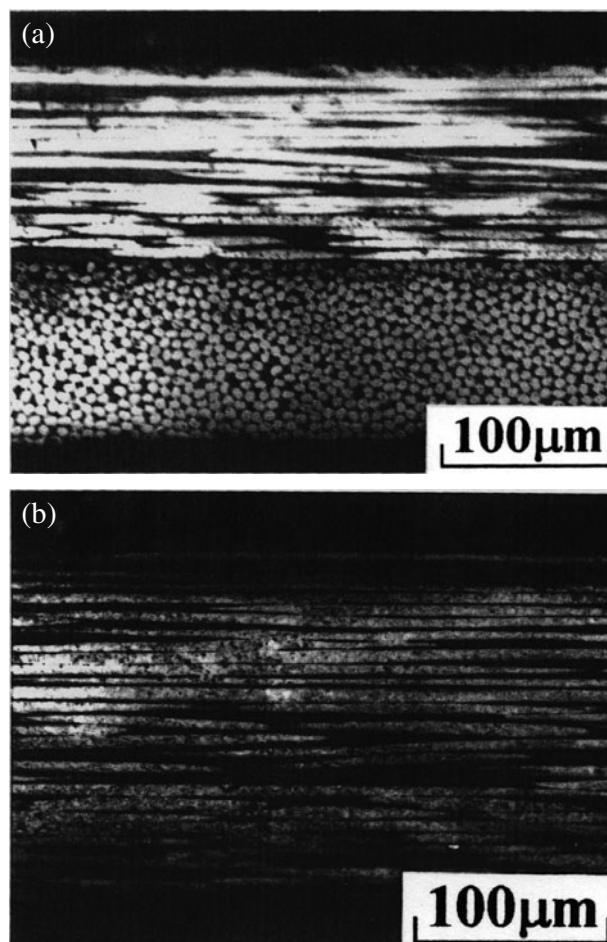


Figure 18. Optical micrographs of the cross-sections of the junctions, showing the two laminae. (a) Crossply, (b) unidirectional.

A conventional thermocouple array can be used to provide spatially resolved temperature sensing. However, a conventional thermocouple array requires much wiring. In addition, the tips of conventional thermocouples must be at or near the outer surface of the composite structure. If the thermocouples are embedded in the composite, they are intrusive and degrade the mechanical properties of the composite. If the thermocouples are attached on the surface of the composite, they can be detached easily. Therefore, in practice, a conventional thermocouple array is not feasible for spatially resolved temperature sensing.

7.2. Thermistor array

7.2.1. Experimental methods. Materials and sample preparation were as described in section 2.2, except that the square junction was of typical size $5 \text{ mm} \times 5 \text{ mm}$. Figure 18(a) shows an optical micrograph of the cross-section of a crossply sample and figure 18(b) shows that of the cross-section of a unidirectional sample. The two laminae could be distinguished in the crossply junction, but not in the unidirectional junction. Every sample consisted of one or more such junctions. During composite fabrication, pressure on the junction(s) was provided by a steel weight. A glass-fiber–epoxy-matrix composite spacer was placed between the weight

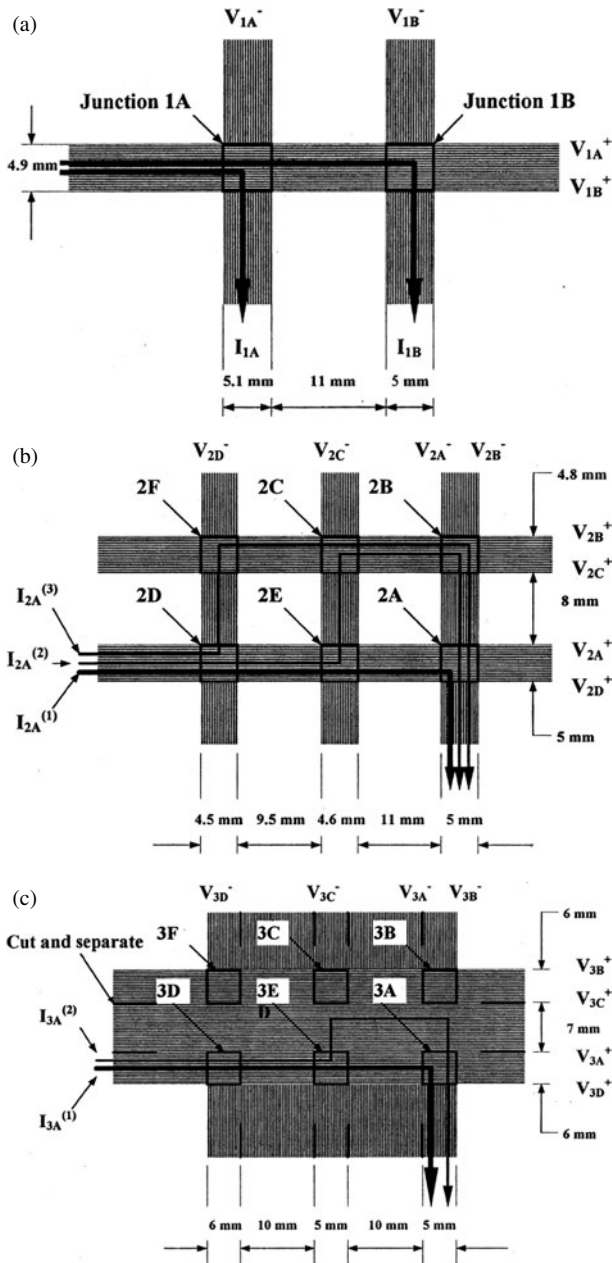


Figure 19. Junction arrays and configurations for measuring the contact resistance. (a) Sample 1, (b) sample 2, (c) sample 3.

and the junction(s) to make sure that the weight was applied to the junction(s) only. Sample 1 (figure 19(a)) had two crossply junctions, labeled 1A and 1B. Sample 2 (figure 19(b)) had six crossply junctions; the contact resistivities of four of the six junctions, labeled 2A, 2B, 2C, and 2D, were measured. Sample 3 (figure 19(c)) had one large crossply junction, which was subdivided into smaller areas by splitting the ends of each of the two lamina strips. The contact resistivities of four of the small areas, labeled 3A, 3B, 3C, and 3D, were measured. Samples 4–8 described below were employed to study the effect of the curing pressure. Sample 4 had two crossply junctions, the pressures on which were respectively 0 and 0.19 MPa during curing. Samples 5–8 had only one junction each. Samples 5–7 were crossply; sample 8 was unidirectional. The pressures on samples 5–8 during curing were 0.062, 0.13, 0.33, and

0.42 MPa, respectively. The samples were put between the two heating platens of a Carver hot press, where they were cured at $148 \pm 2^\circ\text{C}$ for 10.6 h (for samples 1, 2, and 3) or $175 \pm 2^\circ\text{C}$ for 10 h (for samples 5–8). The average heating rate was either $4.4^\circ\text{C min}^{-1}$ (for samples 1–3) or $2.5^\circ\text{C min}^{-1}$ (for samples 4–8). After curing, the samples were furnace (platen) cooled to room temperature; this took about 11 h. Heating using the platens is referred to as hot plate heating.

To test the temperature sensing ability of the junctions that had completed curing, samples 1–3 were heated back to the curing temperature ($148 \pm 2^\circ\text{C}$) at the rate of $4.4^\circ\text{C min}^{-1}$ and then furnace cooled. After that, they were heated to $160 \pm 2^\circ\text{C}$ at the rate of $4.4^\circ\text{C min}^{-1}$ and then furnace cooled. Still after that, they were heated to $105 \pm 5^\circ\text{C}$ (for samples 1 and 2) at the rate of $1.6^\circ\text{C min}^{-1}$ or to $150 \pm 2^\circ\text{C}$ (for sample 3) at the rate of $0.18^\circ\text{C min}^{-1}$, and then furnace cooled. The other samples (samples 4–8) were heated from 50°C to $150 \pm 2^\circ\text{C}$ at the rate of $0.15^\circ\text{C min}^{-1}$ and then cooled at the same rate.

To test the temperature detection ability of the junctions that had completed curing, either an incandescent desk lamp or a tungsten–halogen lamp (100 W) with a blue filter was used to shine light of spot diameter 50 mm on each sample. Unless stated otherwise, the former was used. For samples 1 and 4–8, the light was aimed at the centers of the junctions in turn. For samples 2 and 3, the light spot was at the centers of junctions 2A and 3A, respectively.

During temperature variation or light shining, the contact resistance R_c for each junction of interest was separately measured using the four-probe method, as shown in figure 2(a). The contact resistivity ρ_c was calculated from the equation $\rho_c = R_c A$, where A is the contact (junction) area. In figure 19(a), the current path I_{1B} and the voltage difference $V_{1B}^+ - V_{1B}^-$ are involved in measuring the contact electrical resistivity of junction 1B, whereas the current path I_{1A} and the voltage difference $V_{1A}^+ - V_{1A}^-$ are involved in measuring the contact resistivity of junction 1A. For each resistivity measurement, only one current path is possible. However, in figure 19(b), due to the larger number of fiber groups in each lamina, multiple current paths are involved when the contact resistivity of a junction is measured. For example, the measurement of the contact resistivity of junction 2A involves current paths $I_{2A}^{(1)}$, $I_{2A}^{(2)}$, and $I_{2A}^{(3)}$. Path $I_{2A}^{(1)}$ gives information on junction 2A and path $I_{2A}^{(2)}$ gives information on junctions 2E, 2C, and 2B, whereas path $I_{2A}^{(3)}$ gives information on junctions 2D, 2F, and 2B. Because three contact resistances are involved in either path $I_{2A}^{(2)}$ or $I_{2A}^{(3)}$, whereas only one contact resistance is involved in path $I_{2A}^{(1)}$, path $I_{2A}^{(1)}$ is the path of least resistance. Therefore, $I_{2A}^{(1)}$ is much greater than either $I_{2A}^{(2)}$ or $I_{2A}^{(3)}$. Although $I_{2A}^{(2)}$ and $I_{2A}^{(3)}$ contribute information on junctions that are not under resistivity measurement to the measured resistivity of junction 2A, the contributions are small. Nevertheless, their contributions mean that one junction's contact resistance can affect the measured contact resistance of another junction in a junction array.

Electrical resistance measurement was conducted as described in section 2.2. For a sample with multiple junctions, R_c for each junction was measured separately—one at a time. The time delay between the resistance measurement of two junctions was less than half a second. Hence, all the junctions in a sample were measured at essentially the same time.

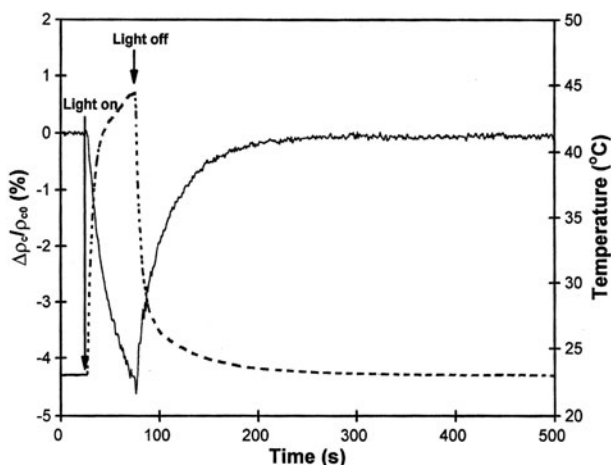


Figure 20. The fractional change in contact resistivity (solid curve) of junction 1A and the temperature (dashed curve), obtained simultaneously during light shining.

The temperature of the samples was continuously measured by one or more T-type thermocouples. A thermocouple was put just beside each of junctions 1A, 2A, and 3A for samples 1, 2, and 3 respectively and just beside each of the junctions for the other samples. The light shining experiments were performed twice under the same conditions for each sample. During the first time, a thermocouple was put just beside the junction being shone. During the second time, the thermocouple was put on the top of the junction center. The temperature difference between the two situations was from 2 to 4 °C. The contact resistance was measured during the first time and the temperature was measured during the second time. To measure the temperature distribution, four thermocouples were put right on the centers of junctions 2A, 2B, 2C, and 2D in the case of sample 2 (3A, 3B, 3C, and 3D in the case of sample 3). To compare the effect of light shining and hot plate heating, after the light shining experiment, each of samples 4–8 was hot plate heated up to the highest temperature reached during prior light shining at $0.5\text{ }^{\circ}\text{C min}^{-1}$, and then furnace cooled. At the same time, the contact resistance was measured.

7.2.2. Results and discussion. Figure 20 shows how the fractional change of contact resistivity ($\Delta\rho_c/\rho_{co}$) and temperature of junction 1A changed when the tungsten-halogen lamp was turned on and then off. When the lamp was turned on, the contact resistivity decreased, while the temperature increased. When the lamp was turned off, the contact resistivity increased while the temperature decreased. The effect was reversible. Figure 21 shows a similar result, but the incandescent lamp used was much weaker. Although the range of temperature change was only about $0.3\text{ }^{\circ}\text{C}$, the change in contact resistivity was detectable.

Figure 22 shows the variation of $\Delta\rho_c/\rho_{co}$ of junction 1A with temperature during hot plate heating and cooling (without shining light). The $\Delta\rho_c/\rho_{co}$ decreased when the temperature increased and $\Delta\rho_c/\rho_{co}$ increased when the temperature decreased; the effect was essentially totally reversible.

The results above indicate that shining light has a strong influence on the contact resistivity, and this influence does not result mainly from the light itself but from the heat effect of

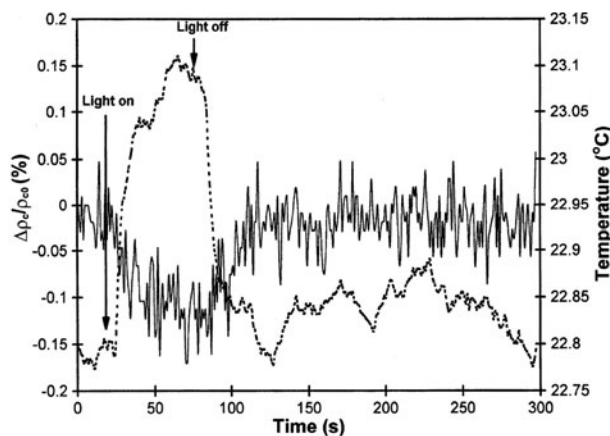


Figure 21. The fractional change in contact resistivity (solid curve) of junction 1A and the temperature (dashed curve), obtained simultaneously during light (weaker than that in figure 20) shining.

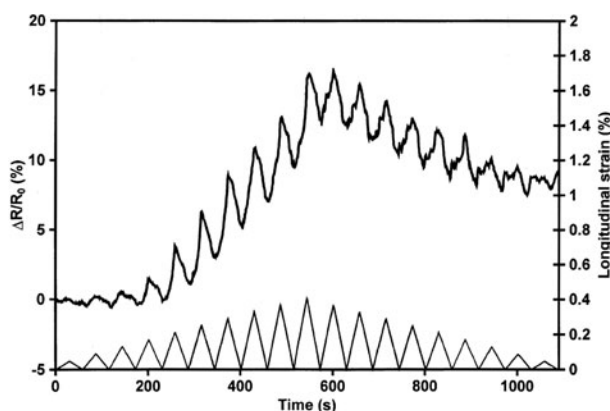


Figure 22. The fractional change in contact resistivity (solid curve) of junction 1A and the temperature (dashed curve) during hot plate heating and cooling without light shining.

the light. That light failed to affect the electrons directly is due to the inability of the light to penetrate the top lamina ($120\text{ }\mu\text{m}$ thick, figure 18(a)) and reach the junction. Table 5 shows the influence of the curing pressure and composite configuration. For the same composite configuration (crossply), the higher the curing pressure, the smaller the pressure exerted by the fibers of one lamina on those of the other lamina at the junction, and the lower the contact resistivity. A higher curing pressure corresponds to a higher fiber volume fraction in the composite. (The fiber volume fractions for the curing pressures of 0.13, 0.33 and 1.4 MPa were measured and found to be 0.50, 0.52 and 0.58 respectively.) During curing and subsequent cooling, the matrix shrinks while the carbon fibers essentially do not, so a longitudinal compressive stress will develop in the fibers. For carbon fibers, the modulus in the longitudinal direction is much higher than that in the transverse direction. Moreover, the fibers are continuous in the longitudinal direction. Thus, the overall shrinkage in the longitudinal direction tends to be less than that in the transverse direction. Therefore, there will be an interlaminar stress in the two crossply layers in a given direction. This stress accentuates the barrier for the electrons to jump from one lamina to the other. The greater the interlaminar stress, the higher the barrier, which is the activation energy. After curing and subsequent cooling, heating will decrease the

Table 5. The influence of curing pressure and composite configuration.

Composite configuration	Curing pressure (MPa)	Composite thickness (mm)	Contact resistivity ρ_{co} (Ω cm ²)	$(\Delta\rho_c/\rho_{co})/\Delta T$ ($^{\circ}\text{C}^{-1}$)	
				Due to light shining (%)	Due to hot plate heating (%)
[0/90] (crossply)	0	0.36	0.73	-0.132	-0.0959
	0.062	0.32	0.14	-0.133	-0.0898
	0.13	0.31	0.18	-0.160	-0.126
	0.19	0.29	0.054	-0.269	-0.179
0.33	0.26	0.0040	-1.10	-0.888	
[0] (unidirectional)	0.42	0.23	0.29	-0.0145	-0.0457

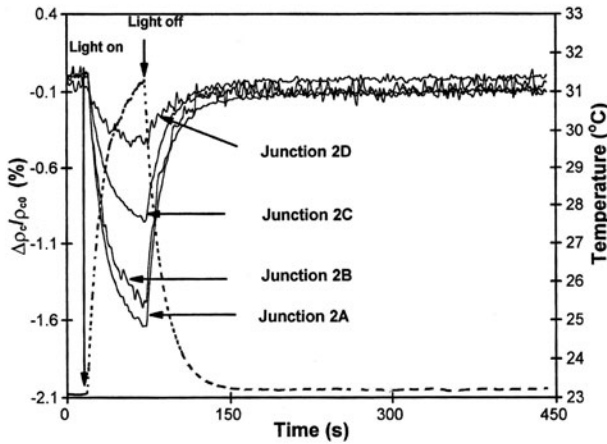


Figure 23. The fractional change in contact resistivity (solid curve) of junction 2A, 2B, 2C, and 2D and the temperature (dashed curve) of junction 2A, obtained simultaneously during light shining. The center of the light spot was at the center of junction 2A. The distance of the centers of 2A, 2B, 2C, and 2D from the center of the light spot was 0, 12.9, 20.4 and 29.9 mm, respectively.

thermal stress, due to the CTE mismatch between fibers and matrix. However, the thermal stress is probably smaller than the curing stress, so the activation energy does not decrease upon heating (section 2). Therefore, the higher the curing pressure, the larger the fiber volume fraction, the greater the interlaminar stress, the higher the activation energy, and the greater the absolute value of the fractional change in contact resistivity/ $^{\circ}\text{C}$.

The fact that this absolute value for the case of shining light is a little higher than that for the case of hot plate heating probably indicates that light has some additional effect on the contact resistivity other than its heat effect. This phenomenon may also be because light shining gave a higher heating rate, less uniformity in temperature, and hence a higher thermal stress.

The curing pressure for the sample in the unidirectional composite configuration was higher than that of any of the crossply samples. Consequently, the thickness was the lowest. As a result, the fiber volume fraction was the highest. However, its contact resistivity was the second highest rather than being the lowest, while the absolute values of $(\Delta\rho_c/\rho_{co})/\Delta T$ were very low compared to the crossply samples. Hence, the difference in composite configuration made a big difference to the contact resistivity and its response to temperature changes. As explained in section 2, the unidirectional configuration gave a higher contact resistivity

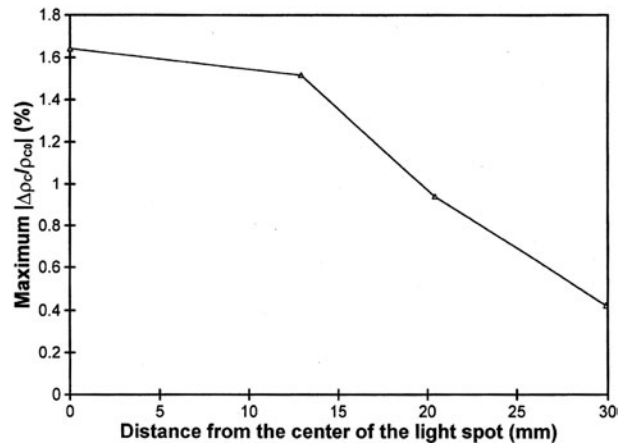


Figure 24. The peak value of the fractional change in contact resistivity as a function of the distance from the center of the light spot.

than the crossply configuration (table 2). In the unidirectional sample, the fibers of one of the laminae sank into the other lamina at the junction, as suggested by figure 18(b), so pressure helped relatively little in the contact between fibers of adjacent laminae.

The very low absolute value of $(\Delta\rho_c/\rho_{co})/\Delta T$ for the unidirectional sample probably resulted from the fact that there was no CTE or curing shrinkage mismatch between the two laminae, so that the interlaminar stress was absent and the energy gap was very low (table 2). The fact that the absolute value of $(\Delta\rho_c/\rho_{co})/\Delta T$ due to light shining was smaller than that due to hot plate heating for the unidirectional sample is yet to be elucidated. Both values for light shining and hot plate heating were much lower than those of the crossply samples. Thus the unidirectional junction was not as effective for light/temperature sensing as the crossply junction.

Figure 23 shows the fractional changes in contact resistivity for junctions 2A, 2B, 2C, and 2D of sample 2 when the light (incandescent) was turned on and off. The center of the light spot was at the center of junction 2A. The distance between the center of the light spot and the center of junction 2A, 2B, 2C, and 2D is 0, 12.9, 20.4 and 29.9 mm, respectively. Figure 24 shows the relationship between the peak magnitude of the fractional contact resistivity change and the distance from the center of the light spot. The temperature distribution given by thermocouples under the same incandescent light source is shown in figure 25. The relationship between the peak temperature change and the distance from the center of the light spot is shown in figure 26.

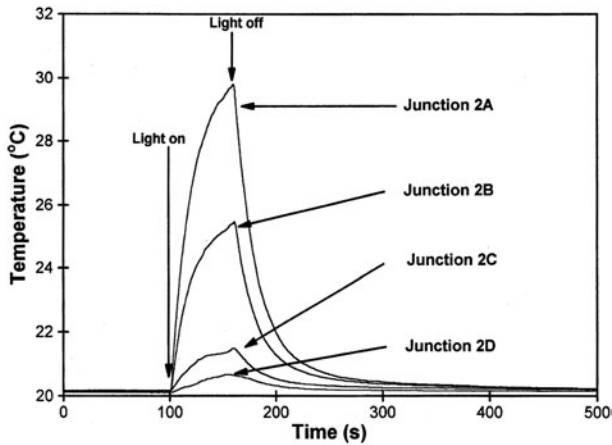


Figure 25. The temperature changes of junctions 2A, 2B, 2C, and 2D during light shining, obtained by putting a thermocouple at the center of each of junctions 2A, 2B, 2C, and 2D.

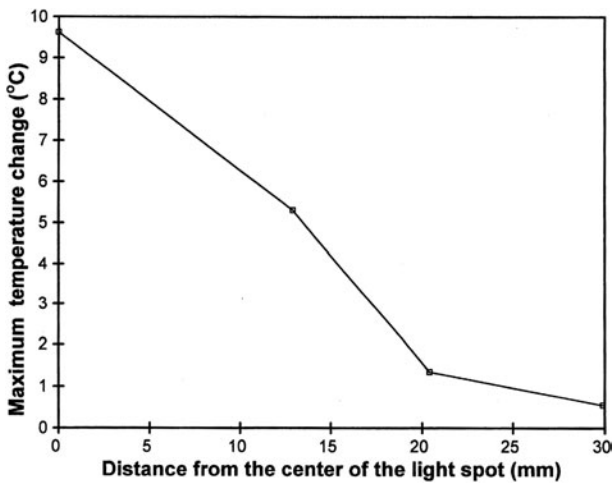


Figure 26. The maximum temperature change as a function of the distance from the center of the light spot.

Figures 23–26 indicate that the nearer we are to the center of the light spot, the greater the magnitude of the fractional contact resistivity change and the greater the temperature change. The contact resistivity decrease is because the temperature increase results in an increase in the number of electrons which are energetic enough to jump from one lamina to the other. The fractional contact resistivity change can be used to locate the light spot, since the difference in $\Delta\rho_c/\rho_{c0}$ between the different positions is large. Comparison among figures 23–26 shows that the values $\Delta\rho_c/\rho_{c0}$ of junctions 2B and 2A (figure 23) are quite close, while the temperatures of these junctions are quite different (figure 25). On the other hand, the changes in $\Delta\rho_c/\rho_{c0}$ of junctions 2C and 2D are quite different (figure 23), but the temperatures of these junctions are quite close (figure 25). Figure 27 shows the relationship between the peak magnitude of the fractional contact resistivity change and the peak temperature change of junctions 2A, 2B, 2C, and 2D. Figure 28 shows the same type of relationship for the single junction of sample 7. The curve is quite linear. However, the curve in figure 27 is not linear. This is because multiple current paths exist in the case of multiple junctions. The measured change in contact resistance of one junction

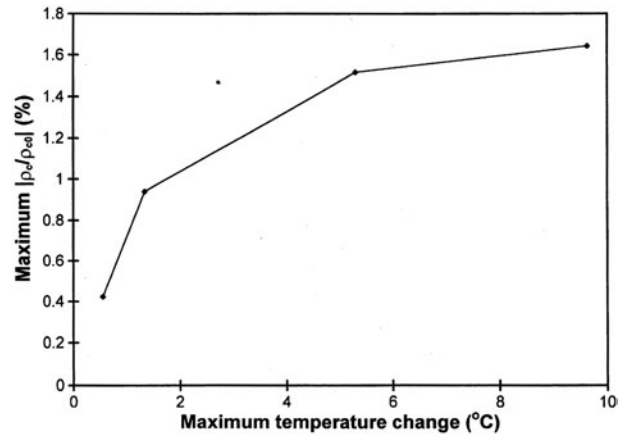


Figure 27. The relationship between the peak absolute value of the fractional change in contact resistivity and the peak value of the temperature change for junctions 2A, 2B, 2C, and 2D.

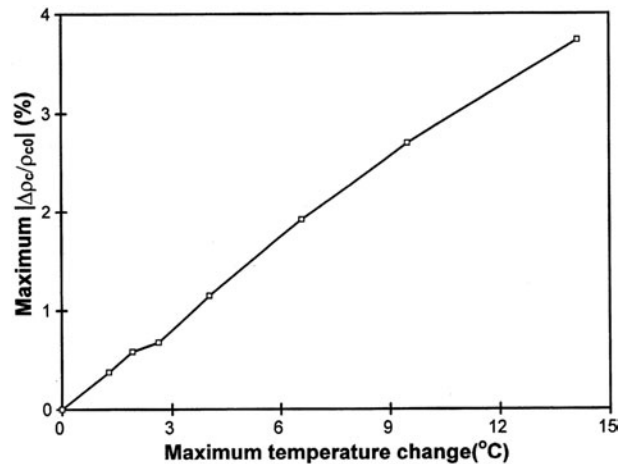


Figure 28. The relationship between the peak absolute value of the fractional change in contact resistivity and the peak value of the temperature change for the single junction of sample 7.

is affected by the change in contact resistance of the other junctions. For the case of multiple junctions, the greater the temperature change, the more gradual was the increase of the peak fractional contact resistivity change; the sensitivity was good when the temperature change was less than 6°C.

Similar results for sample 3 are shown in figure 29. Sample 3 gave a similar distribution of fractional contact resistivity change as sample 2 (figure 23). The configuration of sample 3 is closer to the situation of practical application than that of sample 2. The similarity of the results of samples 2 and 3 means that the fiber groups of adjacent junctions do not need to be separated by a gap in practical application.

7.2.3. Conclusion for section 7.2. An epoxy-matrix continuous carbon-fiber composite comprising two crossply laminae was found to be a temperature sensor, which could be used as a light sensor. Each junction between crossply fiber groups of the adjacent laminae was a sensor, while the fiber groups served as electrical leads. A junction array allowed temperature/light distribution sensing. The contact electrical resistivity of the junction decreased reversibly upon heating, due to the electron hopping between the laminae. The

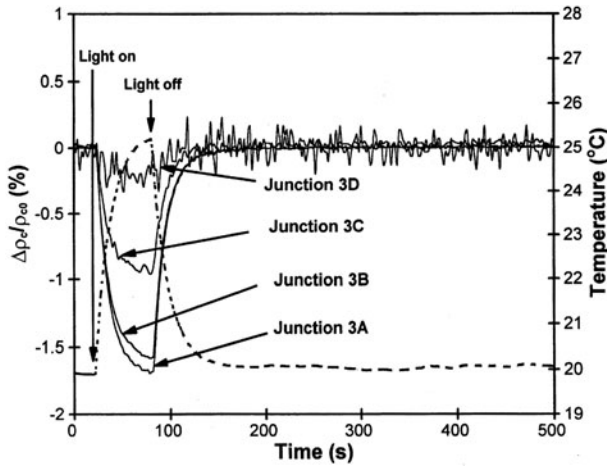


Figure 29. The fractional changes in contact resistivity (solid curve) of junctions 3A, 3B, 3C, and 3D and the temperature (dashed curve) of junction 3A, obtained simultaneously during light shining. The center of the light spot was at the center of junction 3A. The distances of the centers of 3A, 3B, 3C, and 3D from the center of the light spot were 0, 13.0, 19.8 and 30.5 mm, respectively.

fractional change in contact resistivity provided an indication of temperature/light. The contact resistivity decreased with increasing pressure during composite fabrication, due to increase in pressure exerted by fibers of one lamina on those of the other lamina. The magnitude of the fractional change in contact resistivity/°C increased with increasing curing pressure. A crossply junction is much better than a unidirectional junction as a temperature/light sensor, due to the absence of interlaminar stress in the latter.

7.3. Thermocouple array

7.3.1. *Experimental methods.* The materials and composite preparation are as described in section 6. A sample with six crossply junctions of P-25 and T-300 (figure 30) was made to measure the temperature distribution. The curing procedure of the sample was the same as that of the single junction involving T-300 prepreg except that the curing pressure was 0.25 MPa.

7.3.2. *Results and discussion.* The six-junction sample (figure 30) can be used as a simple thermocouple array. Each of the junctions is a thermocouple, thus allowing temperature distribution sensing. Figure 31 shows the temperature distribution during light shining measured by conventional thermocouples. The temperature decreased from junction A to D, for the distance to the center of the light spot increases from A to D. Corresponding to the temperature distribution, we have the voltage distributions, as shown in figure 32. Figure 32(a) shows the voltage distribution for voltage probe configuration I. It is quite consistent with the temperature distribution, since configuration I minimizes the influences of the other junctions on the voltage of the junction to be measured. However, the voltage distribution measured by configuration II (figure 32(b)) is less consistent with the temperature distribution, especially for junctions C and D. This is because of the mutual influences of the junction. Both configurations I and II indicate correctly the junction with the highest temperature.

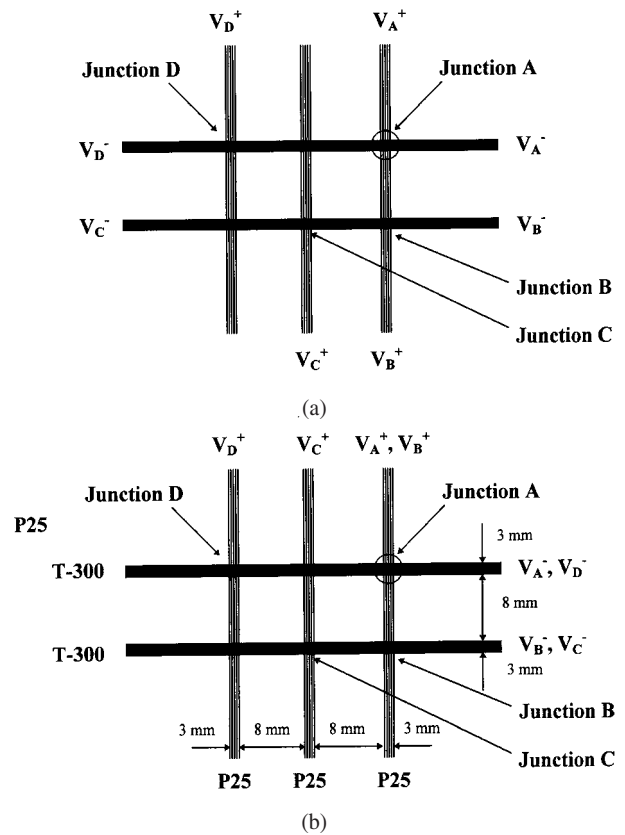


Figure 30. A six-junction sample for temperature distribution sensing, each of the junctions comprising pristine P-25 and pristine T-300. The center of the light spot was at junction A. (a) Voltage probe configuration I. (b) Voltage probe configuration II.

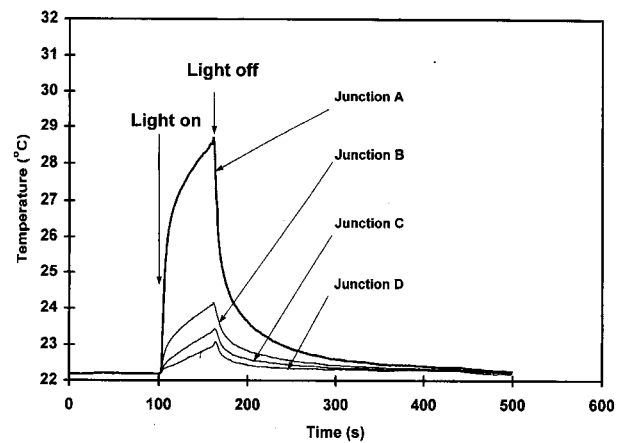


Figure 31. Variation of the temperatures of junctions A, B, C, and D of the six-junction sample during light shining. The center of the light spot was at junction A.

7.4. Conclusion for section 7

A polymer- (epoxy-) matrix composite with the top two laminae of continuous carbon fibers in a crossply configuration is a temperature sensor. The temperature sensor is a thermistor if the laminae comprise similar fibers and is a thermocouple if the laminae comprise dissimilar fibers. Each junction between crossply fiber groups of adjacent laminae is a sensor, while the fiber groups serve as electrical leads. A junction array provided

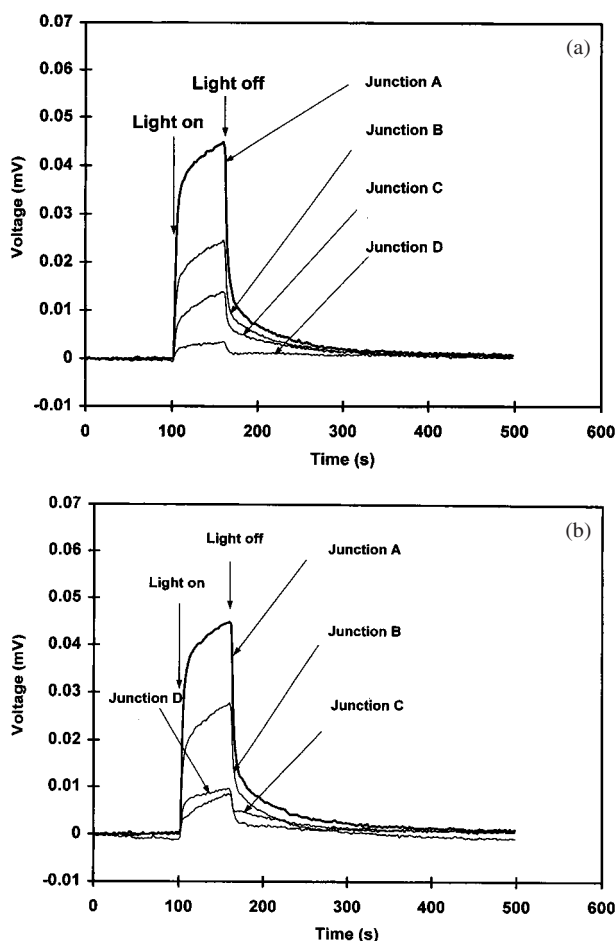


Figure 32. Variation of the voltages of junctions A, B, C, and D of the six-junction sample during light shining. (a) Voltage probe configuration I. (b) Voltage probe configuration II.

by two crossply laminae allows sensing of the temperature distribution. A junction between unidirectional fiber groups of adjacent laminae is much less effective as a thermistor, due to the absence of interlaminar stress.

8. Conclusion for this paper

The use of the interlaminar interface as a sensor is an approach which was found to be effective in continuous carbon-fiber-epoxy-matrix composites for sensing temperature, moisture, and damage. In the case of temperature sensing, the interlaminar interface functioned as either a thermistor or a thermocouple junction. The thermocouple approach required the fibers in the contacting laminae to be dissimilar, whereas the thermistor approach did not.

The thermistor function was provided by the contact electrical resistivity of the interlaminar interface decreasing reversibly with increasing temperature, with an activation energy of 0.12 eV for a crossply configuration. The activation energy was much lower for the unidirectional configuration.

The thermocouple function was provided by dissimilar carbon fibers in the adjacent laminae, the junction of which was the thermocouple junction. A thermocouple sensitivity of $82 \mu\text{V } ^\circ\text{C}^{-1}$ was attained by using graphitic (Thornel P-100) carbon fibers that had been intercalated with bromine

and sodium. The thermocouple sensitivity was the same for unidirectional and crossply junctions.

The moisture sensing function was provided by the contact electrical resistivity of the interlaminar interface increasing reversibly with increasing humidity, due to moisture uptake at the interface.

The stress sensing function was provided by the contact electrical resistivity of the interlaminar interface decreasing upon compression in the direction perpendicular to the interface. The effect was much larger and much more repeatable for a thermoplastic-matrix (nylon-6) composite than a thermoset-matrix (epoxy) composite. The effect was essentially reversible for the thermoplastic-matrix composite, but was partially reversible for the thermoset-matrix composite.

The damage sensing function was provided by the contact electrical resistivity of the interlaminar interface increasing upon damage. During thermal damage sensing, simultaneous temperature sensing was provided by the thermistor function.

By using two crossply laminae, a two-dimensional array of sensors was attained and demonstrated to be effective for temperature distribution sensing.

References

- [1] Sugita M, Yanagida H and Muto N 1995 *Smart Mater. Struct.* **4** A52-7
- [2] Prabhakaran R 1990 *Exp. Tech.* **14** 16-20
- [3] Ceysson O, Salvia M and Vincent L 1996 *Scr. Mater.* **34** 1273-80
- [4] Kaddour A S, Al-Salehi F A R and Al-Hassani S T S 1994 *Compos. Sci. Technol.* **51** 377-85
- [5] Schulte K and Baron Ch 1989 *Compos. Sci. Technol.* **36** 63-76
- [6] Schulte K 1993 *J. Physique IV* **3** 1629-36
- [7] Abry J C, Bochart S, Chateauminois A, Salvia M and Giraud G 1999 *Compos. Sci. Technol.* **59** 925-35
- [8] Todoroki A, Kobayashi H and Matsuura K 1995 *JSME Int. J. A* **38** 524-30
- [9] Irving P E and Thiagarajan C 1998 *Smart Mater. Struct.* **7** 456-66
- [10] Wang X and Chung D D L 1996 *Smart Mater. Struct.* **5** 796-800
- [11] Wang X and Chung D D L 1997 *Smart Mater. Struct.* **6** 504-8
- [12] Wang X and Chung D D L 1997 *Polym. Compos.* **18** 692-700
- [13] Wang X and Chung D D L 1998 *Composites B* **29B** 63-73
- [14] Wang X and Chung D D L 1998 *Compos. Interfaces* **5** 191-9
- [15] Wang X, Fu X and Chung D D L 1998 *J. Mater. Res.* **13** 3081-92
- [16] Wang X, Fu X and Chung D D L 1999 *J. Mater. Res.* **14** 790-802
- [17] Wang X and Chung D D L 1997 *Carbon* **35** 1649-51
- [18] ASTM Standard 1995 D 2344-84 pp 43-5
- [19] Zhou G, Green E R and Morrison C 1995 *Compos. Sci. Technol.* **55** 187-93
- [20] Iyer S L, Sivaramakrishnan C and Young C 1989 *Proc. 34th Int. SAMPE Symp.* (Covina, CA: SAMPE) pp 2172-81
- [21] Blythe A R 1980 *Electrical Properties of Polymers* (Cambridge: Cambridge University Press)
- [22] Selzer R and Friedrich K 1997 *Composites A* **28** 595
- [23] Wood C A and Bradley W L 1997 *Compos. Sci. Technol.* **57** 1033
- [24] Crasto A S and Kim R Y 1997 *Proc. 1995 6th Symp. on Composites: Fatigue and Fracture* (Conshohocken, PA: ASTM) p 381 (ASTM Special Publication)
- [25] Asp L E 1998 *Compos. Sci. Technol.* **58** 967
- [26] Todo M, Nakamura T and Takahashi K 2000 *J. Compos. Mater.* **34** 630

- [27] Selzer R and Friedrich K 1995 *J. Mater. Sci.* **30** 334
- [28] Pratt B A and Bradley W L 1997 *Proc. 1995 Symp. on High Temperature and Environmental Effects on Polymeric Composites* (Conshohocken, PA: ASTM) p 64 (ASTM Special Publication)
- [29] Zhao S and Gaedke M 1996 *Adv. Compos. Mater.* **5** 291
- [30] Tsotsis T K and Lee S M 1997 *J. Reinf. Plast. Compos.* **16** 1609
- [31] Biro D A, Pleizier G and Deslandes Y 1993 *Compos. Sci. Technol.* **46** 293
- [32] Karasek M L, Strait L H, Amateau M F and Runt J P 1995 *J. Compos. Technol. Res.* **17** 3
- [33] Ogi K, Kim H S, Maruyama T and Takao Y 1999 *Compos. Sci. Technol.* **59** 2375
- [34] Soutis C and Turkmen D 1997 *J. Compos. Mater.* **31** 832
- [35] Adams R D and Singh M M 1996 *Compos. Sci. Technol.* **56** 977
- [36] Buehler F U and Seferis J C 2000 *Composites A* **31** 741
- [37] Schmid R 1986 *Proc. 7th Int. Conf. of the Society for the Advancement of Process Engineering European Chapter (Mater. Sci. Monographs 35)* (Amsterdam: Elsevier) p 311
- [38] Chou P J C and Ding D 2000 *J. Thermoplast. Compos. Mater.* **13** 207
- [39] Ogi K and Takeda N 1997 *J. Compos. Mater.* **31** 530
- [40] Dispennette J M, Seng L, Jang B Z and Linton R C 1994 *50 Years of Progress in Materials Science and Technology, Proc. 26th Int. SAMPE Tech. Conf.* vol 26 (Covina, CA: SAMPE) p 119
- [41] Shim H H, Kwon O K and Youn J R 1992 *Wear* **157** 141
- [42] Woo E M 1994 *Composites* **25** 425
- [43] Lai J-Y and Young K-F 1995 *Compos. Struct.* **30** 25
- [44] Hough J A, Xiang Z D and Jones F R 1998 *Key Eng. Mater.* **144** 27
- [45] Wu Y-J, Chung K, Takatoya T, Bruce C and Seferis J C 1999 *Int. SAMPE Symp. Exhibition* vol 44 (Covina, CA: SAMPE) p 773
- [46] Armistead J P and Snow A W 1996 *Proc. 1994 Symp. on Fiber Matrix and Interface Properties* (Conshohocken, PA: ASTM) p 168 (ASTM Special Tech. Pub.)
- [47] Zhuang H and Wightman J P 1997 *J. Adhes.* **62** 213
- [48] Lu Y, Xue G, Wu F and Wang X 1996 *J. Adhes. Sci. Technol.* **10** 47
- [49] Aniskevich A N and Yanson Y O 1991 *Mech. Compos. Mater.* **26** 455
- [50] Wang S and Chung D D L 1999 *Compos. Interfaces* **6** 497
- [51] Wang S and Chung D D L 2000 *J. Mater. Sci.* **35** 91
- [52] Wang S and Chung D D L 1999 *Composites B* **30** 591
- [53] Wang S and Chung D D L 2001 *Polym. Polym. Compos.* **9** 135
- [54] Chung D D L 2001 *Polym. Compos.* **22** 250
- [55] Herokovich C T and Hyer M Q 1985 *Eng. Fract. Mech.* **25** 779–91
- [56] Allix O, Bahlouli N, Cluzel C and Perret L 1996 *Compos. Sci. Technol.* **56** 883–8
- [57] Allix O, Bahlouli N, Ladeveze P and Perret L 1994 *Damage Mech. Compos. Am. Soc. Mech. Eng.* **185** 21–35
- [58] Huang X, Gillespie J W Jr and Eduljee F R 1997 *Composites B* **28B** 419–24
- [59] Crasto A S and Kim R Y 1993 *J. Reinf. Plast. Compos.* **12** 545–58
- [60] Dutta P K 1997 *Proc. Int. Offshore Polar Engineers Conf.* vol 4, pp 672–6
- [61] Mosallam A and Dutta P K 2001 *Proc. Int. Offshore and Polar Engineering Conf.* vol 4 (Stavanger, Norway: Norske Conoco) pp 211–7
- [62] Wang X and Chung D D L 1997 *Polym. Compos.* **18** 692–700
- [63] Wang X and Chung D D L 1998 *Composites B* **29B** 63–73
- [64] Wang X, Wang S and Chung D D L 1999 *J. Mater. Sci.* **34** 2703–14
- [65] Schulte K 1993 *J. Physique Coll. IV* **3** C7 1629–36
- [66] Schulte K and Baron Ch 1989 *Compos. Sci. Technol.* **36** 63–76
- [67] Prabhakaran R 1990 *Exp. Tech.* **14** 16–20
- [68] Herokovich C T and Hyer M Q 1985 *Eng. Fract. Mech.* **25** 779–91
- [69] Augh L, Gillespie J W Jr and Fink B K 2001 *J. Thermoplastic Compos. Mater.* **14** 96–115
- [70] Crasto A S and Kim R Y 1993 *J. Reinf. Plast. Compos.* **12** 545–58
- [71] Kallmeyer A R and Dutta P K 2004 *Int. J. Offshore Polar Eng.* **13** 232–9
- [72] di Vittorio S L, Dresselhaus M S, Endo M, Issi J-P, Piroux L and Bayot V 1991 *J. Mater. Res.* **6** 778–83
- [73] Kuriyama K and Dresselhaus M S 1991 *J. Mater. Res.* **6** 1040–7
- [74] Tsukamoto J, Takahashi A, Tani J and Ishiguro T 1989 *Carbon* **27** 919–23
- [75] Stokes K L, Tritt T M, Fuller-Mora W W, Ehrlich A C and Jacobsen R L 1996 *Proc. ICT'96: 15th Int. Conf. on Thermoelectrics (Pasadena, CA, 1996)* pp 164–7
- [76] Sun M, Li Z, Mao Q and Shen D 1998 *Cem. Concr. Res.* **28** 549–54
- [77] Ho C T and Chung D D L 1990 *Carbon* **28** 825–30
- [78] Gupta V, Mathur R B, Bahl O P, Marchand A and Flandrois S 1995 *Carbon* **33** 1633–9
- [79] Wessbecher D E, Forsman W C and Gaier J R 1998 *Synth. Met.* **26** 185–94
- [80] Hérolde C, Hérolde A and Lagrange P 1996 *J. Phys. Chem. Solids* **57** 655–62
- [81] Gaier J R, Hamburger P D and Slabe M E 1991 *Carbon* **29** 313–20
- [82] Gaier J R, Davidson M L and Shively R K 1996 *Technology Transfer in a Global Community (Int. SAMPE Tech. Conf. vol 28)* (Covina, CA: SAMPE) pp 1136–47
- [83] Katsumata M, Endo M, Yamanashi H and Ushijima H 1994 *J. Mater. Res.* **9** 1829–33